

1 **Anonymous Referee #1**

2
3 *This paper from Karydis et al. predicts fine particle acidity, which is an important aerosol property*
4 *linked to many particulate physicochemical processes, on the global scale and over a long historic*
5 *period of 50 years. It discovers some interesting longterm trends in particle acidity with discussions on*
6 *seasonal variabilities. Most importantly, it highlights the important roles of alkaline salts, such as*
7 *ammonium and crustal cations, to buffer and elevate the global pH. The results are of interest to the*
8 *geoscience community and supported by high-quality modeling, thus suitable for the scope of ACP*
9 *Letter. However, several issues should be clarified before acceptance for publication, especially the*
10 *large discrepancies in pH prediction (in some cases more than 2 units) when compared to*
11 *observationally-constrained pH in previously reported studies, since the overestimation of pH results in*
12 *exaggerating the importance of alkaline salts and the accuracy of pH prediction determines its*
13 *implications to atmospheric chemistry.*

14
15 We would like to thank the reviewer for his/her positive response and for the very thoughtful review.
16 By raising important issues, the reviewer helped us further to better present our results and improve the
17 manuscript. Below is a point by point response on the comments and suggestions.

18
19 **Major comments**

20
21 **1.** *Line 50 & Line 218: the assumption of aerosol mode (solid+liquid vs. liquid) matters for pH*
22 *prediction. For instance, it changes the estimated pH by more than 3 units in Pasadena. The current*
23 *text in the method section lacks the explanation why the stable mode was chosen over metastable mode.*
24 *More discussions would be useful to validate the model results. The Pasadena pH estimation in Guo et*
25 *al. (2017) assumes metastable aerosols due to the high RH observed in that study ($79 \pm 17\%$).*
26 *Considering the even higher RH after sunset, particles are highly likely to get deliquesced and stay so*
27 *even in the daytime when RH drops below DRH (deliquescence relative humidity) but above ERH*
28 *(efflorescence relative humidity). Such an effect would be observed in a place with a similar RH diurnal*
29 *cycle. I wonder if a better way to present the model results is to choose the metastable mode for high*
30 *RH cases/regions (such as the average RH of 60% and with nighttime/max RH over mutual DRH) and*
31 *the stable mode for low RH cases/regions, especially when the two results deviate from each other by*
32 *more than one pH unit. But the key judgment is which particle-phase assumption works the best to*
33 *predict gas-particle partitioning of semi-volatile species comparing to observations (while the particle*
34 *phase measurement/modeling is not available on the global scale).*

35
36 We agree with the reviewer that the aerosol state assumption is important for the pH calculations with
37 ISORROPIA and needs further attention in our manuscript. Here we used a revised ISORROPIA-II
38 model which includes modifications proposed by Song et al. (2018), who resolved coding errors related
39 to pH calculations when the stable state assumption is used. Applying the revised model during winter
40 haze events in Beijing, they have found that the assumed particle phase state, either stable or metastable,
41 does not significantly impact the pH predictions. However, a sensitivity simulation in our study (e.g.,
42 applying both stable and metastable assumptions on a global scale) revealed that even if the assumed

Formatted

43 particle phase state does not significantly impact the pH calculations over oceans and polluted regions
44 (i.e., characterized by high RH values), the metastable assumption produces more acidic particles (up to
45 2 units of pH) in regions affected by high concentrations of crustal cations (i.e., downwind of desert
46 areas) and consistently low RH values. Fountoukis et al. (2007) have shown that the metastable solution
47 predicts significant amounts of water below the mutual DRH (MDRH, where all salts are
48 simultaneously saturated with respect to all components). In addition, the presence of high calcium
49 concentrations downwind of the deserts results in increasing pH values due to the missing precipitation
50 of insoluble salts such as the CaSO_4 . This is something that the metastable state assumption fails to
51 reproduce since it treats only the ions in the aqueous phase. In general, high amounts of crustal species
52 can significantly increase the aerosol pH which is consistent with the presence of excess carbonate in
53 the aerosol phase (Meng et al., 1995). Since our model is applied on a global scale, we believe that the
54 stable state assumption can reproduce the sensitivities of pH more accurately given that the focus of our
55 manuscript is on insights regarding the impacts of alkaline species on aerosol acidity. The stable state
56 assumption gives almost identical results with the metastable in areas with high NH_3 concentrations
57 (e.g., over central Europe) and at the same time is more appropriate for regions affected by crustal
58 elements (i.e., close to deserts). Overall, the stable state assumption used here as a basecase simulation
59 produces about 0.5 units higher global average pH than the metastable assumption.

60 Polluted areas that are downwind of crustal sources (like Pasadena) are of special interest and will be
61 discussed more elaborately in the manuscript. When calculating species concentrations, the stable state
62 solution algorithm of ISORROPIA II starts with assuming a completely dry aerosol and based on the
63 ambient RH dissolves each of the salts depending on their DRH. However, in the ambient atmosphere,
64 when the RH over a wet particle is decreasing, the wet aerosol may not crystallize below the MDRH but
65 instead remain in a metastable state affecting the uptake of water by the aerosol and thus the pH. We
66 agree with the reviewer that this can happen in some locations with high diurnal variations of RH.
67 However, over Pasadena, the observed RH is always high ($87 \pm 9\%$) for the period used for our model
68 comparison (second half of the campaign where $\text{PM}_{2.5}$ were measured). Our sensitivity analysis
69 revealed that the aerosol state was not affected by the state assumption since over Pasadena, both stable
70 and metastable assumptions predict the same amount of water in the aerosol. We believe that the
71 differences on pH are due to the high concentrations of calcium from the Great Basin Desert which
72 results in the precipitation of high amounts of CaSO_4 , lowering the particle acidity (but without
73 affecting the water activity since CaSO_4 is insoluble and does not contribute to the MDRH depression).
74 It is worth mentioning that calcium was not included in the Guo et al. (2017) study which can explain
75 the differences in the observed and simulated aerosol acidity. Our sensitivity analysis shows that the
76 simulated particle-phase fraction of nitrate over Pasadena is 40% using the stable state assumption and
77 32% using the metastable assumption, compared to the observed 51%. This is in accordance with the
78 findings of Ansari and Pandis (2000) who suggested that the stable state results in higher concentrations
79 of aerosol nitrate when the RH is low ($<35\%$) and/or sulfate to nitrate molar ratios are low (<0.25).
80 Karydis et al. (2016) have shown that while the aerosol state assumption has a marginal effect on the
81 calculated nitrate aerosol tropospheric burden (2% change), it can be important over deserts at very low
82 RHs where nitrate is reduced by up to 60% by using the metastable assumption.

83
84

85 2. Table S1 summarizes the comparison of simulated fine particle pH in this study to
86 observationally-constrained pH in previous studies. In most cases, the simulated pH is higher, and the
87 differences range from sub-one units up to six units. It is acknowledged that some previous estimations
88 are biased low for lack of gas-phase input (e.g., Line 76). However, large differences are seen when
89 compared to some observationally-constrained pH with gas-phase input, such as Pye et al. (2018) (7.0
90 vs. 1.1) and Murphy et al. (2017) (4.2 vs. 1.6). Also, the prediction of remote air in the Atlantic and
91 Pacific Oceans (roughly 5-6 in Figure 1 other than lower values of 3 predicted for the northern parts
92 that are heavily affected by anthropogenic emissions) is much higher than pH estimations based on
93 ATom aircraft studies (roughly 0-1) (Nault et al., 2020). Although the ATom estimations are based on
94 submicron particles (and this study focuses on PM_{2.5}), it is hard to believe that sea salts or mineral
95 dust between 1 and 2.5 μm can elevate particle pH by 4-7 units on average. In summary, the results are
96 very different, such as nearly neutral vs. highly acidic fine particles (i.e., very different implications for
97 chemistry), requiring more discussions on the causes (e.g., crustal elements, mixing state, or particle
98 phase). Possibilities include 1) that the simulated crustal elements may be externally mixed with
99 sulfate/nitrate/ammonium aerosols or 2) the overestimation of crustal elements or the sum of ammonia
100 and ammonium. In either case, the effects of alkaline compounds on the global fine particle acidity
101 would be less than proposed. One way to tell the key factor(s) is by comparing the thermodynamic
102 model inputs between the simulated ones and the field observations and do some sensitivity tests.

103

104 The calculation of aerosol acidity on a global scale requires the advanced treatment of atmospheric
105 aerosol chemical complexity, analogous to the real atmosphere and beyond the conventional methods
106 used by the current chemistry-climate models (CCM). The atmospheric chemistry model system EMAC
107 is the ideal tool for this purpose since it is one of the most comprehensive CCM containing advanced
108 descriptions of the aerosol thermodynamics (including the dust-pollution interactions) and organic
109 aerosol formation and atmospheric aging (affecting the aerosol water). Therefore, the comprehensive
110 global atmospheric multiphase chemistry simulations of the past 50 years presented in this study
111 enabled us for the first time to provide accurate aerosol acidity calculations and the associated
112 sensitivities. Our model calculations for aerosol acidity are based on several important processes/factors
113 that are not included explicitly, or usually neglected, by model calculations used to constrain the aerosol
114 acidity from observations. These are the following:

115

116 1/ As discussed above, the stable/metastable assumption does not affect the simulated pH most of the
117 time, however, in some case with low RHs and the presence of crustal cations, the metastable
118 assumption results in lower pHs.

119 2/ Crustal species from surrounding deserts and Na⁺ from sea salt can elevate the pH significantly in
120 some locations, however, these are often neglected from observations.

121 3/ The organic aerosols (which are treated comprehensively by our model using the module
122 ORACLE and the volatility basis set framework) can contribute significantly to the aerosol water, and
123 thus increase the aerosol pH. This contribution is not considered by many observational studies.

124 4/ The inclusion of gas phase species (e.g., NH₃, HNO₃) in the pH calculations is important, since
125 using only the aerosol-phase as input (i.e., reverse mode) the inferred pH exhibits a bimodal behavior
126 with very acidic or alkaline values depending on whether anions or cations are in excess (Hennigan et

127 al., 2015). Even if the forward mode is used (without gas phase input), the calculated aerosol pH is
128 biased low (approximately 1 unit of pH) due to the repartition of semivolatile anions (i.e., NH_3) to the
129 gas phase to establish equilibrium (Guo et al., 2015).

130 5/ Another important aspect, usually not mentioned in many studies, relates to the methods used to
131 derive the campaign-average (or for 3D models the simulated average) pH. In our model the aerosol pH
132 is calculated online (2-minute time resolution), while output is stored every five hours based on
133 instantaneous concentrations of fine aerosol H_2O and H^+ . According to Jensen's inequality (Jensen,
134 1906), the average of the instantaneous pH values is less than or equal to the pH calculated based on the
135 average of the H_2O and H^+ instantaneous values. We estimate that the average pH calculated based on
136 5-hourly instantaneous values is approximately 1-3 (~2 globally averaged) units higher than the pH
137 calculated based on the average H_2O and H^+ concentrations. If other models are using average values
138 (and not instantaneous) as output, or if field-derived pH calculations are using average observed H_2O
139 and H^+ values, this can result in important underestimations of aerosol pH.

140 6/ Some unrealistically high pH values in a few past studies resulted from coding errors in the stable
141 state assumption of ISORROPIA II model, which have been fixed in our study following the
142 recommendation of Song et al. (2018).

143 7/ The type of thermodynamic model used is also important. Song et al. (2018) has found that
144 ISORROPIA-II produces somewhat higher pH (by 0.1-0.7 units, negatively correlated with RH)
145 compared to the thermodynamic model E-AIM, which is used to observationally-constrain pH in some
146 studies.

147 8/ Measurements of $\text{PM}_{2.5}$ nitrate are not always reliable because of artifacts associated with the
148 volatility of ammonium nitrate (Schaap et al., 2004). Ammonium and nitrate can partially evaporate
149 from Teflon filters at temperatures between 15 to 20 °C and can evaporate completely at temperatures
150 above. The evaporation from quartz filters is also significant at temperatures higher than 20 °C. This
151 systematic underestimation of ammonium nitrate can affect the observed chemical composition of the
152 aerosol and thus the pH calculations.

153 9/ A final important issue refers to the comparison between global model output and observations at
154 specific locations. This also concerns the aerosol concentrations but is especially important for a
155 tentative property like the aerosol acidity. Apart from the size of our grid cells (which is $1.9^\circ \times 1.9^\circ$), the
156 altitude is also important. Our model has a first layer which is approximately 67m in height. On the
157 other hand, ground observations are typically collected in a height up to 3 m. While the aerosols within
158 size modes simulated in our model are well-mixed, perhaps this is not the case for the aerosols observed
159 so close to the surface and potentially to sources, and thus the aerosol acidity may be higher (e.g., due to
160 the higher contribution from local primary sources like SO_4^{2-} , lower water in the aerosol, or lower
161 semivolatile cations like NH_4^+)
162

163 All the above points are now extensively discussed in the manuscript. Concerning the comparison
164 with observationally derived pH from aircraft campaigns, we need to emphasize that all pH values
165 reported in our study are near the surface and cannot be directly compared to aircraft campaigns. Every
166 aerosol size mode in our model is well mixed while the size modes are externally mixed. Therefore, we
167 agree with the reviewer that our crustal elements are in many cases externally mixed with sulfates and
168 ammonium but nitrates do exist in our large particles as well since they condense to the coarse (and

169 accumulation) mode particles in order to maintain the charge balance in the aerosol phase. However, the
170 aerosol pH of PM_{2.5} is calculated based on the total H₂O and H⁺ in the aerosol until the cut-off point of
171 2.5 μm in our aerosol lognormal distributions. Our model predicts important amounts of crustals and
172 Na⁺ in the PM_{1-2.5} size range, therefore the pH of PM_{2.5} is meaningfully higher than that of PM₁. Finally,
173 it is worth mentioning that Nault et al. (2020) did not include Na⁺ in their suit of components.

174
175 **3.** *Caution should be paid towards Ca (especially for the cases of high Ca mass concentrations)*
176 *due to the precipitation of CaSO₄ as ISORROPIA-II assumes it to be completely insoluble. Some*
177 *sensitivity tests may be carried out such as done in Kakavas et al. (2021).*

178
179 This indeed is a critical point as discussed earlier in our response for the case of Pasadena. Calcium is
180 the major crustal component of dust in most deserts (Karydis et al., 2016) and unlike Mg, K, and Na it
181 can react with sulfate ions and form insoluble CaSO₄, which precipitates out of the aerosol aqueous
182 phase. This interaction reduces the aqueous sulfate and thus the aerosol acidity. In our sensitivity
183 simulation without crustal component emissions, this effect is evident in the western United States and
184 East Asia where high concentrations of sulphate interact with strong emissions of calcium emitted from
185 the Great Basin and the Gobi deserts, respectively, resulting in the increase of pH by up to two units
186 (Figure 1 of the manuscript). The role of CaSO₄ in this sensitivity response is now emphasized in the
187 revised text.

188
189 **4.** *Line 26: Please elaborate on how the cited papers show the effects of aerosol acidity on particle*
190 *hygroscopic growth and its lifetime. The three papers talk about the importance of mineral dust in*
191 *thermodynamic modeling. For example, Karydis et al. (2016) highlight that the tropospheric nitrate*
192 *burden increases by 44% when considering dust aerosol chemistry but the connection between aerosol*
193 *acidity to hygroscopicity or lifetime seems to be buried.*

194
195 We agree with the reviewer that the Karydis et al. (2016) study focuses more on the thermodynamic
196 interactions between mineral dust anions and inorganic cations and their impact on nitrate aerosol
197 formation. In the revised text we have replaced this study with the Karydis et al. (2017) work where the
198 impacts of these thermodynamic interactions on aerosol hygroscopicity and cloud droplet formation are
199 revealed.

200
201 **5.** *Line 66: “The aerosol pH over the anthropogenically-influenced northern hemispheric mid-*
202 *latitudes exhibits a clear seasonal pattern with lower values during boreal summer and higher ones*
203 *during winter, driven by the availability of ammonium and by the aerosol water content (Fig. 2).” First,*
204 *please specify the locations after “northern hemispheric mid-latitudes”. Second, it is not clear these*
205 *regions exhibit clear seasonal variations as stated. For instance, the curves of the eastern US and*
206 *Europe are nearly flat throughout the year, while the western US shows lower pH in the winter months*
207 *(e.g., Dec, Jan, and Feb), opposite to the trends stated in the text*

209 This is correct. Not every region of the Northern Hemisphere exhibits this behavior. This is mostly
210 evident over highly polluted regions like East Asia and not over Europe and Eastern USA. The Northern
211 extratropical Oceans also show the same clear seasonal pattern. We have corrected the text accordingly.
212

213 **6.** *Line 101: Suggest rephrasing the sentence as “Over North America, aerosol acidity also*
214 *decreased with reduced SO₂ and NO_x emissions.” However, it seems to be more complicated for NO_x*
215 *than SO₂, since more total nitrate may increase pH given the same amount of sulfate, transferring*
216 *aerosols from a more acidic ammonium sulfate (or ammonium bisulfate) system to a less acidic*
217 *ammonium nitrate system.*
218

219 The SO₂ emissions over North America have decreased more steeply compared to the NO_x emissions.
220 However, even if this was not the case, the reduction of NO_x alone cannot affect the sulfate
221 concentrations (by replacing it with nitrates in the aerosol). The available sulfuric acid condenses
222 instantaneously onto the aerosol phase and form ammonium sulfate (or ammonium bisulfate) and only
223 then the nitric acid can form ammonium nitrate with the free NH₃ left.
224

225 **7.** *Line 118: The dominant H₂O₂ pathway at pH < 5 is for cloud droplets, not fine particles.*
226 *Cheng et al. (2016) state that the NO₂ pathway dominates at pH > 5 and the TMI pathway (transition*
227 *metal ions) dominates at pH < 4.5 for the Beijing haze conditions. So even if the authors chose to only*
228 *calculate the H₂O₂ pathway (which is probably the most important one for the less polluted cases at pH*
229 *< 5) for the past 50 years, it is worth mentioning the other possible dominant pathway.*
230

231 What we have calculated in our work is the O₃ pathway which is important for both cloud droplets
232 and aerosols for pH above 5 units. However, we agree with the reviewer that the reference to the H₂O₂
233 pathway in the text is misleading, and now we refer to the other important SO₂ oxidation pathways in
234 the aqueous aerosol phase (e.g., NO₂ above pH=5 and TMI below pH=5).
235

236 **8.** *Line 131: Stating that NH₃ is a major buffer is reasonable since it is often found in both gas and*
237 *particle phases. Thus, it can redistribute between the two phases to buffer the pH. It remains to be*
238 *explained though if the crustal elements simply increase particle pH or buffer the pH since they are*
239 *non-volatile. For instance, although carbonate or bicarbonate is not considered in the ISORROPIA-II*
240 *calculation, it could be the anion paired with crustal elements to buffer high pH for the H₂CO₃ pKa of*
241 *6.4 (The pKa of HCO₃⁻ is 10.3, which is too high to buffer the predicted pH predicted in this study).*
242

243 Overall, in the text we refer to the buffering capacity of crustal elements as a term to describe their
244 activity to decrease the pH of the aerosol with respect to an increase in the acid concentrations (i.e.,
245 owing to the anthropogenic activities). We recognize that the term is not completely accurate since
246 crustal cations are non-volatile and can only increase the pH (and not buffer it). Following the
247 reviewer’s comment, we have revised the text accordingly.
248

249 **9.** *Line 211: It would be useful to specify if the kinetic limitations affect simulations in this study*
250 *and by what extent. The thermodynamic simulations based on observations often don’t find the signs of*

251 kinetic limitations for fine particles (i.e., the predicted gas-particle partitioning agrees with
252 observations, e.g. (Guo et al., 2017; Liu et al., 2017)), unless very fresh aerosols are sampled near the
253 sources.

254

255 The assumption of thermodynamic equilibrium is a good approximation for fine-mode aerosols that
256 can reach equilibrium very fast. However, the equilibrium timescale for large particles is typically
257 larger than the time step of the model (Meng and Seinfeld, 1996) leading to errors in the size
258 distribution of semi-volatile ions like nitrate. Since the current study include reactions of nitric acid with
259 coarse sea-salt and dust aerosol cations, the competition of fine and coarse particles for the available
260 nitric acid can only be accurately represented by taking into account the kinetic limitations during
261 condensation of HNO_3 in the coarse mode aerosols. This information has been added to the text.

262

263 **10.** Line 267: It is not clear why Equation A2 is used to investigate the impact of pH on nitrate
264 partitioning but not the results directly from ISORROPIA. The two should be equivalent. Please explain.

265

266 Indeed, equation A2 is in theory equivalent with the instant calculations of ISORROPIA II within our
267 global model EMAC. However, the output of our model is not every timestep (is every 5 hours), and
268 only after every other process in the model is calculated. Therefore, if we use the model output (e.g.,
269 gas-phase HNO_3 and NO_3^- in 4 size modes) the result would be subject to uncertainties from other
270 processes (e.g., deposition, coagulation, transport, etc.). The use of Eq. 2 can provide us a clearer
271 picture of the impact of pH on HNO_3 gas/particle partitioning. We have added this information in the
272 text.

273

274 **Minor comments**

275

276 **1.** Line 31: Consider deleting “In the past” and changing the past form to present form since the
277 ion balance and molar ratio methods still have these limitations and also don’t consider the partial
278 disassociation of acids, which could be added here.

279

280 Thank you for pointing this out. We have revised the sentence accordingly.

281

282 **2.** Line 56: Change “high pH’s are found. . .” to “high pH are found”.

283

284 Done.

285

286 **3.** Line 78: Add “(Fig. 1)” after the sentence “Over the Arctic and the northern Atlantic and
287 Pacific Oceans, aerosol acidity is significantly enhanced by strong sulfur emissions from international
288 shipping and pollution transport from industrialized areas.” Since the former and latter sentences are
289 talking about Fig. 2.

290

291 Thank you for the suggestion.

292

293 **4.** *Line 90: Does it make sense to have the most points in Fig. S1 with larger than one cation/anion*
294 *ratios? Not for liquid only particles but reasonable for solid+liquid aerosols. So it would be great to*
295 *explain this better either in the main text or in Fig. S1 caption.*

296

297 Yes, the cation/anion ratio include all ions from both solid salts and the liquid phase. This is now
298 explained in the text.

299

300 **5.** *Line 96: Provide kappa for ammonium sulfate and ammonium nitrate.*

301

302 The kappa hygroscopicity parameters for ammonium sulfate and ammonium nitrate are 0.53 and 0.67,
303 respectively. The information has been added to the text.

304

305 **6.** *Fig. 1 caption: Add “during the period 1970-2020” after “Surrounding panels show the*
306 *temporal pH evolution at locations defined in Table 1” to specify the time range (although it can be*
307 *easily told from the panels).*

308

309 The sentence has been revised as “Surrounding panels show the temporal pH evolution during the
310 period 1970-2020 at locations defined in Table 1.”

311

312 **7.** *Line 126: do you mean “overestimate”? Since the SO2 emission reduces drastically in Asia, the*
313 *inventories are not updated in time to catch the reductions. Therefore, I would think overestimation*
314 *makes more sense here logically.*

315

316 We meant that inventories tend to underestimate the real trends (reductions) in emissions. Admittedly,
317 this was quite confusing and now we have rewritten the sentence as “SO₂ emission trends since 2007
318 have been so drastic that inventories and scenarios tend to overestimate the emitted SO₂.”

319

320 **8.** *Line 128: consider change “the large SO2 trends” to “the significant SO2 reduction trends” or*
321 *“the long-term SO2 trends”.*

322

323 Done.

324

325 **9.** *Line 154: add “is” after “NH3” to be “NH3 is also proved to be. . .”*

326

327 Done.

328

329 **10.** *Line 237: consider adding a reference for $\kappa = 0.14$. Also, while the Greek alphabet of κ is*
330 *used here, “kappa” is used in Fig. 4. Better to be consistent.*

331

332 Done.

333 **References:**

334

335 Ansari, A. S., and Pandis, S. N.: The effect of metastable equilibrium states on the partitioning of nitrate
336 between the gas and aerosol phases, *Atmospheric Environment*, 34, 157-168, 10.1016/s1352-
337 2310(99)00242-3, 2000.

338 Cheng, Y., Zheng, G., Wei, C., Mu, Q., Zheng, B., Wang, Z., Gao, M., Zhang, Q., He, K., Carmichael,
339 G., Poschl, U., and Su, H.: Reactive nitrogen chemistry in aerosol water as a source of sulfate during
340 haze events in China, *Sci. Adv.*, 2, e1601530, doi: 10.1126/sciadv.1601530, 2016.

341 Guo, H., Liu, J., Froyd, K. D., Roberts, J. M., Veres, P. R., Hayes, P. L., Jimenez, J. L., Nenes, A., and
342 Weber, R. J.: Fine particle pH and gas–particle phase partitioning of inorganic species in Pasadena,
343 California, during the 2010 CalNex campaign, *Atmos. Chem. Phys.*, 17, 5703-5719, doi:
344 10.5194/acp-17-5703-2017, 2017.

345 Kakavas, S., Patoulias, D., Zakoura, M., Nenes, A., and Pandis, S. N.: Size-resolved aerosol pH over
346 Europe during summer, *Atmos. Chem. Phys.*, 21, 799-811, doi: 10.5194/acp-21-799-2021, 2021.
347 Karydis, V. A., Tsimpidi, A. P., Pozzer, A., Astitha, M., and Lelieveld, J.: Effects of mineral dust on
348 global atmospheric nitrate concentrations, *Atmos. Chem. Phys.*, 16, 1491-1509, doi: 10.5194/acp-16-
349 1491-2016, 2016.

350 Karydis, V. A., Tsimpidi, A. P., Pozzer, A., Astitha, M., and Lelieveld, J.: Effects of mineral dust on
351 global atmospheric nitrate concentrations, *Atmos. Chem. Phys.*, 16, 1491-1509, 10.5194/acp-16-
352 1491-2016, 2016.

353 Karydis, V. A., Tsimpidi, A. P., Bacer, S., Pozzer, A., Nenes, A., and Lelieveld, J.: Global impact of
354 mineral dust on cloud droplet number concentration, *Atmospheric Chemistry and Physics*, 17, 5601-
355 5621, 10.5194/acp-17-5601-2017, 2017.

356 Liu, M., Song, Y., Zhou, T., Xu, Z., Yan, C., Zheng, M., Wu, Z., Hu, M., Wu, Y., and Zhu, T.: Fine
357 particle pH during severe haze episodes in northern China, *Geophys. Res. Lett.*, 44, 5213-5221, doi:
358 10.1002/2017gl073210, 2017.

359 Meng, Z. Y., Seinfeld, J. H., Saxena, P., and Kim, Y. P.: Atmospheric gas-aerosol equilibrium .4.
360 Thermodynamics of carbonates, *Aerosol Science and Technology*, 23, 131-154, 1995.

361 Meng, Z. Y., and Seinfeld, J. H.: Time scales to achieve atmospheric gas-aerosol equilibrium for
362 volatile species, *Atmospheric Environment*, 30, 2889-2900, 10.1016/1352-2310(95)00493-9, 1996.

363 Murphy, J. G., Gregoire, P. K., Tevlin, A. G., Wentworth, G. R., Ellis, R. A., Markovic, M. Z., and
364 VandenBoer, T. C.: Observational constraints on particle acidity using measurements and modelling
365 of particles and gases, Faraday Discuss., 200, 379-395, doi: 10.1039/c7fd00086c, 2017.
366 Nault, B. A., Campuzano-Jost, P., Day, D. A., Jo, D. S., Schroder, J. C., Allen, H. M., et al.: Models
367 underestimate the increase of acidity with remoteness biasing radiative impact calculations, AGU
368 Fall Meeting, doi: <https://agu.confex.com/agu/fm20/meetingapp.cgi/Paper/746418>, 2020.
369 Pye, H. O. T., Zuend, A., Fry, J. L., Isaacman-VanWertz, G., Capps, S. L., Appel, K. W., Foroutan, H.,
370 Xu, L., Ng, N. L., and Goldstein, A. H.: Coupling of organic and inorganic aerosol systems and the
371 effect on gas-particle partitioning in the southeastern US, Atmos. Chem. Phys., 18, 357-370, doi:
372 10.5194/acp-18-357-2018, 2018.
373 Schaap, M., van Loon, M., ten Brink, H. M., Dentener, F. J., and Builtjes, P. J. H.: Secondary inorganic
374 aerosol simulations for Europe with special attention to nitrate, Atmos. Chem. Phys., 4, 857-874,
375 10.5194/acp-4-857-2004, 2004.
376 Song, S., Gao, M., Xu, W., Shao, J., Shi, G., Wang, S., Wang, Y., Sun, Y., and McElroy, M. B.: Fine-
377 particle pH for Beijing winter haze as inferred from different thermodynamic equilibrium models,
378 Atmos. Chem. Phys., 18, 7423-7438, 10.5194/acp-18-7423-2018, 2018.

379
380

381 ***Anonymous Referee #2***

382
383

384 *This paper uses a model to predict fine particle ($PM_{2.5}$) pH globally. They find more acidic particles*
385 *in the more anthropogenically-influenced regions and basic particles in regions of high non-volatile*
386 *cations, a finding that is not highly surprising but which does provide a general verification of the*
387 *method. Their major finding is on how alkaline compounds control $PM_{2.5}$ particle acidity and these*
388 *trends over the past 50 years.*

389

390 We thank the reviewer for his/her review of our manuscript and the helpful comments. Below is a
391 point by point response to his/her comments.

392

393 *The devil is in the details and this is especially true when assessing aerosol particle pH and particle*
394 *pH impacts. As noted by the 1st reviewer, the pH predicted by the model is off by a wide margin in some*
395 *locations relative to predictions supported by data. I would note that the model is often significantly off*
396 *in locations where the pH predictions have been assessed through comparisons between observed*
397 *gas/particle partitioning of HNO_3 and NH_3 to predicted values and where partitioning of at least of*
398 *these species is sensitive to pH, meaning there is high confidence in the pH reported for these cases.*
399 *The first reviewer provided significant details on this issue. I will not repeat those suggestions and*
400 *instead look at a broader view.*

401 *I calculate that the mean (median) pH difference (simulated – field derived) from the data provided*
402 *in Table S1 is 1.61 (1.4), suggesting the model is systematically predicting a high pH globally (the*
403 *authors may wish to check my calculations).*

404 *I suggest the authors spend more time on first making sure, and discussing in more detail, the quality*
405 *of the pH predictions. What causes this high pH bias compared to other reported studies and what are*
406 *the implications. A greater focus on this apparent discrepancy is important since this manuscript is*
407 *based only on a model prediction and incorrectly predicted pH has significant ramifications. First, a*
408 *major finding reported is on the role of alkaline species that raises the particle pH; a high bias pH*
409 *would indicate that the role of alkaline species is overstated in this analysis. Second, the paper also*
410 *focuses on the partitioning of HNO₃, which is highly non-linear with pH, where HNO₃ can change*
411 *from all in the gas phase to all in the particle phase over a change in pH of about 1 to 2 units, near the*
412 *level of the mean difference found in the comparison, as noted above. Thus, the bias could have a large*
413 *impact on this finding as well. Overall, it is not clear what new contribution this paper makes on*
414 *understanding aerosol pH. Substantial modification based on a better assessment of the model should*
415 *be required prior to consideration for publication.*

416
417 As discussed in response to the second comment by the first reviewer, the calculation of aerosol
418 acidity on a global scale requires the advanced treatment of atmospheric aerosol chemical complexity,
419 analogous to the real atmosphere and beyond the conventional methods used by the current chemistry-
420 climate models (CCM). The atmospheric chemistry model system EMAC is the ideal tool for this
421 purpose since it is one of the most comprehensive CCM containing advanced descriptions of the aerosol
422 thermodynamics (including the dust-pollution interactions) and organic aerosol formation and
423 atmospheric aging (affecting the aerosol water). Therefore, the comprehensive global atmospheric
424 multiphase chemistry simulations of the past 50 years presented in this study enabled us for the first
425 time to provide advanced aerosol acidity calculations and the associated sensitivities. Our model
426 calculations for aerosol acidity are based on several important processes/factors that are not included
427 explicitly, or usually neglected, by most of the model-calculations used to constrain the aerosol acidity
428 from observations, and this leads to higher pH values in our analysis. In brief, these factors are the
429 following and are further analyzed in our response to the first reviewer: 1/ the stable/metastable
430 assumption, 2/ The lack of crustal species in the observations, 3/ the omission of the organic aerosols
431 contribution to the aerosol water, 4/ The use of the reverse mode of ISORROPIA, or the lack of gas
432 phase species (e.g., NH₃, HNO₃) in the pH calculations, 5/ Uncertainties on the methods used to derive
433 the campaign-average (or for 3D models the simulated average) pH, 6/ Coding errors in the stable state
434 assumption of ISORROPIA II model in past studies, 7/ The type of thermodynamic model used (e.g., E-
435 AIM vs. ISORROPIA), 8/ Measurement artifacts associated with the volatilization of ammonium nitrate
436 from filters, 9/ The mixing state of aerosol due to the location and height of observational samples
437 compared to the well-mixed aerosols from our model with grid size 1.9°x1.9° and ~67m height.

438
439 *Aside, I do not see the seasonality in mid N American latitudes (noted in lines 67-68, Fig 2), which*
440 *also seems to disagree with two independent observational studies (Wong et al, 2020; Tao et al, 2019)*
441 *and which has significant implications.*

442

443 This is correct. A clear seasonal pattern is mostly evident over highly polluted regions like East Asia
444 and not over Europe and Eastern USA. The Northern extratropical Oceans also exhibit seasonality. We
445 have corrected the text accordingly.

446

447 *Tao, Y., and J. G. Murphy. 2019. 'The sensitivity of PM2.5 acidity to meteorological parameters and*
448 *chemical composition changes: 10-year records from six Canadian monitoring sites', *Atm. Chem.**
449 *Phys., 19: 9309-20.*

450 *Wong, J. P. S., Y. Yang, T. Fang, J. A. Mulholland, A. Russell, S. Ebel, A. Nenes, and R. J. Weber.*
451 *2020. 'Fine particle iron in soils and road dust is modulated by coal-fired power plant sulfur', *Envir.**
452 *Sci Technol., 54: 7088-96.*

453

454

455

456

457

458

459

460

461

462

463

464 **How alkaline compounds control atmospheric aerosol acidity**

465 Vlassis A. Karydis^{1,2*}, Alexandra P. Tsimpidi^{1,2,3}, Andrea Pozzer^{1,4}, and Jos Lelieveld^{1,5}

466

467 ¹Max Planck Institute for Chemistry, Atmospheric Chemistry Dept., Mainz, 55128, Germany.

468 ²Forschungszentrum Jülich, Inst. for Energy and Climate Research, IEK-8, Jülich, 52425, Germany.

469 ³National Observatory of Athens, Inst. for Environmental Research and Sustainable Development, Athens, 15236, Greece.

470 ⁴International Centre for Theoretical Physics, Trieste, 34151, Italy

471 ⁵The Cyprus Institute, Climate and Atmosphere Research Center Nicosia, 1645, Cyprus.

472

473 *Correspondence to:* Vlassis A. Karydis (v.karydis@fz-juelich.de)

474 **Abstract.** The acidity of atmospheric aerosols regulates the particulate mass, composition and toxicity, and has important
475 consequences for public health, ecosystems and climate. Despite these broad impacts, the global distribution and evolution
476 of aerosol acidity are unknown. We used the ~~particular~~, comprehensive atmospheric multiphase chemistry – climate model
477 EMAC to investigate the main factors that control aerosol acidity, and uncovered remarkable variability and unexpected
478 trends during the past 50 years in different parts of the world. We find that alkaline compounds, notably ammonium, and to a
479 lesser extent crustal cations, ~~buffer~~regulate the aerosol pH on a global scale. Given the importance of aerosols for the
480 atmospheric energy budget, cloud formation, pollutant deposition and public health, alkaline species hold the key to control
481 strategies for air quality and climate change.

482 1. Introduction

483 Aerosol acidity is a central property of atmospheric particulates that influence clouds, climate and air quality, including
484 impacts on human health (Raizenne et al., 1996;Lelieveld et al., 2015). It affects the partitioning of semi-volatile acids
485 between the gas and aerosol phases (Guo et al., 2016;Guo et al., 2017;Guo et al., 2018;Nenes et al., 2020), secondary organic
486 aerosol (SOA) formation (Xu et al., 2015;Marais et al., 2016), the solubility of trace metals in aerosols (~~Oakes et al.,~~
487 ~~2012~~)(Oakes et al., 2012), associated with their toxicity (~~Fang et al., 2017~~)(Fang et al., 2017) and nutrient capacity (Jickells
488 et al., 2005), the activation of halogens that act as oxidants (Saiz-Lopez and von Glasow, 2012), the conversion of sulfur
489 dioxide (Seinfeld and Pandis, 2006;Cheng et al., 2016), the particle hygroscopic growth and lifetime (Metzger et al.,
490 2006;Abdelkader et al., 2015;Karydis et al., ~~2016~~2017), and atmospheric corrosivity (Leygraf et al., 2016). Direct
491 measurement of aerosol acidity is difficult and associated with much uncertainty, being dependent on filter sampling and the
492 H⁺ molality in the aqueous extract, which is sensitive to artifacts (~~Pathak et al., 2004~~)(Pathak et al., 2004). Therefore, particle
493 pH, a commonly used acidity metric of aqueous aerosols, is typically inferred by proxy techniques (Hennigan et al.,
494 2015;Pye et al., 2020). Two of the most common are the ion balance and the molar ratio methods. ~~In the past, these~~These
495 methods ~~did~~do not consider the effects of aerosol water and multiphase interactions with gas phase species ~~as well as the~~
496 ~~partial dissociation of acids~~ (Hennigan et al., 2015). The simultaneous measurement of gas phase species can improve
497 aerosol pH estimates by accounting for the phase partitioning of semi-volatile species (e.g., NH₃, HNO₃). However, the
498 accuracy of this approach relies on the availability of information on these species in both the gas and aerosol phase, being
499 scant in most cases.

500 The ~~best~~most reliable estimates of pH are obtained with thermodynamic equilibrium models, although the accuracy can
501 be limited by not accounting for all ionic species. For example, most atmospheric chemistry models do not consider crustal
502 elements (e.g., Ca²⁺, Mg²⁺, K⁺, ~~Na⁺~~) ~~and Na⁺ in sea salt~~. These species affect the ion balance by influencing the phase
503 partitioning of nitrate and ammonium, especially in areas where aeolian dust is abundant (Karydis et al., 2016). Here we
504 present 50-year global acidity trends of fine aerosols (i.e. with a diameter < 2.5 μm) by employing the EMAC chemistry –
505 climate model (Jöckel et al., 2010). The pH calculations are performed online with the ISORROPIA II thermodynamic
506 equilibrium model (Fountoukis and Nenes, 2007).

507 2. Results and Discussion

508 2.1 Global variability of aerosol acidity

509 Figure 1 shows the modeled near-surface distribution of fine aerosol acidity for the 2010-2015 period. We find
510 predominantly acidic particles over the anthropogenically influenced regions in the northern hemisphere and the tropical
511 biomass burning zones, and mostly alkaline particles over deserts and oceans, especially over the southern oceans. The pH
512 typically ranges from 4.0 to 6.7 (5.3 on average) over the western USA since it is affected by crustal cations from the
513 surrounding deserts. ~~Therefore, Polluted areas located downwind of crustal sources are of special interest since~~ the pH
514 calculations ~~in this region are can be~~ sensitive to the aerosol state assumption. ~~(see section 4.3)~~. Over Pasadena, the base case

515 model using the stable state mode estimates a mean pH of 5.9 units, while the sensitivity simulation with only liquid aerosols
516 results in 2.7 pH units (equal to Guo et al. (2017) estimations by using the metastable assumption; Table S1). Our sensitivity
517 analysis revealed that the aerosol state itself is not affected by the state assumption since both stable and metastable predict
518 the same amount of water in the aerosol. Differences in the calculated pH can be due to the high concentrations of calcium
519 from the Great Basin Desert which results in the precipitation of high amounts of CaSO₄, lowering the particle acidity (but
520 without affecting the water activity since CaSO₄ is insoluble and does not contribute to the MDRH depression). It is worth
521 mentioning that calcium was not included in the Guo et al. (2017) study which helps explain the differences in the observed
522 and simulated aerosol acidity. The simulated particle-phase fraction of nitrate over Pasadena is 40% using the stable state
523 assumption and 32% using the metastable assumption, compared to the observationally derived 51%. Over Europe, the pH
524 ranges from 2.6 to 6.7 (3.9 on average). Observational estimates of aerosol pH from the Po Valley (Squizzato et al.,
525 2013; Masiol et al., 2020) and Cabauw (Guo et al., 2018) support the relatively low acidity of fine aerosols over Europe
526 (Table S1). Model calculations compare well with observational estimates from Cabauw, however, result in higher pH (~1
527 unit) compared to values from Po Valley (estimated by using the E-AIM model). Over East Asia the average pH is 4.7,
528 ranging from 2.6 to 7.4. Relatively high $pH^* - spH$ are found over regions where anthropogenic aerosols are mixed with
529 aeolian dust, e.g., from the Gobi Desert, which bufferdecrease the acidity (e.g., ~6 pH units over Hohhot, which agrees well
530 with the estimations of Wang et al. (2019a)). The relatively low pH in large parts of Asia is explained by strong SO₂
531 emissions and associated sulfate, which have increased strongly in the past decades (e.g., over Guangzhou, supported by
532 estimations of Jia et al. (2018)). Estimates of unrealistically high aerosol acidity can result from omitting the gas phase
533 concentrations of semi-volatile ions from the pH calculations (e.g., estimates over Hong Kong (Yao et al., 2007; Xue et al.,
534 2011), Singapore (Behera et al., 2013) and Shanghai (Pathak et al., 2009); Table S1). At the same time, SO₂ emissions have
535 decreased over Europe and USA, and recently in China. However, aerosols over the eastern USA have remained acidic, with
536 an average pH of 3.0 until recently, corroborating the findings of Weber et al. (2016) and Lawal et al. (2018) that aerosol
537 acidity over this region is less sensitive to SO₂ than to NH₃ emissions.

538 The aerosol pH over the anthropogenically-influencedpolluted northern hemispheric mid-latitudes (e.g., over East Asia)
539 and the northern extratropical oceans exhibits a clear seasonal pattern with lower values during boreal summer and higher
540 ones during winter, driven by the availability of ammonium and by the aerosol water content (Fig. 2). This is evident from
541 both our model calculations and from observational estimates mostly in heavily populated areas such as the Po Valley
542 (Squizzato et al., 2013), Beijing (Tan et al., 2018), and Tianjin (Shi et al., 2017), and to a lesser extent over areas strongly
543 affected by aeolian dust (e.g., Hohhot; Wang et al., 2019b) (Table S1). Over tropical regions, fine particulates have a pH
544 between 3.2 and 7.4, being strongly influenced by pyrogenic potassium, i.e., from widespread biomass burning (Metzger et
545 al., 2006), and a high aerosol water content. Observational estimates from Sao Paulo support these high pH values (Vieira-
546 Filho et al., 2016), albeit with 1 unit bias mainly related to the use of the E-AIM model. Over deserts, aerosols are relatively
547 alkaline, with a pH up to 7.4. Aerosols in the marine environment tend to be alkaline also, with a pH up to 7.4 over the
548 southern oceans. Observational estimates report highly acidic aerosols over the southern oceans due to the lack of gas phase
549 input for the pH calculations (Dall'Osto et al., 2019). Over the Arctic and the northern Atlantic and Pacific Oceans, aerosol
550 acidity is significantly enhanced by strong sulfur emissions from international shipping and pollution transport from
551 industrialized areas (Fig. 1). The pH over the northern extratropical oceans and the Arctic ranges from 2.0 to 7.0 with an
552 average of about 5.2. The annual cycle of aerosol acidity over these regions is strongly influenced by anthropogenic

553 pollution, being relatively high during boreal summer. Over the Antarctic, aerosol pH ranges from 4.5 to 7.0 and follows a
554 clear seasonal pattern (Fig. 2).

555 2.2 Temporal evolution of aerosol acidity

556 Figure 1 and Table 1 present the aerosol pH over the period 1970-2020. We investigated the impacts of alkaline species by
557 omitting the emissions of ammonia and mineral cations in two sensitivity simulations.

558 2.2.1 Europe

559 Over Europe, the pH has increased strongly from about 2.8 during the 1970s to 3.9 recently. Especially during the 1990s
560 NH₃ emissions over Europe increased significantly by 14%, while at the same time NO_x and SO₂ emissions decreased by
561 13% and 49%, respectively. While this trend has continued in the past decade, pH changes slowed because the sulfate and
562 nitrate decreases have been compensated through volatilization of ammonia from the particles. In addition, the recently
563 increasing cation/anion ratio is accompanied by a reduction of aerosol water, preventing a significant decrease of the aerosol
564 acidity (Fig. S1). Overall, the increase of aerosol pH by more than 1 unit during the last 50 years had a significant impact on
565 the gas-particle partitioning of semi-volatile acids, e.g., nitric acid, since their dissociation into ions enhances their solubility
566 (Nah et al., 2018). Here, the fraction of nitrate in the particle phase relative to total nitrate (gas plus particle) has increased
567 from ~70% to 85% (Fig. 3). The increase in aerosol pH has been accompanied by an increase in aerosol κ
568 hygroscopicity (Fig. 4). After the substantial reduction of SO₂ emissions, sulfate salts (e.g., ammonium ~~sulphate~~sulfate with
569 $\kappa=0.53$) are replaced by more hygroscopic nitrate salts (e.g., ammonium nitrate with $\kappa=0.67$) in the aerosol
570 composition. In addition, the decrease of organic compound emissions during the last 50 years contributed to the increase of
571 the aerosol hygroscopicity. Our sensitivity simulations reveal that aerosol acidity over Europe is highly sensitive to NH₃
572 emissions. Despite the decline of both SO₂ and NO_x during the past decades, the aerosol would have remained highly acidic
573 (pH ~1) in the absence of NH₃.

574 2.2.2 North America

575 Over North America, aerosol acidity also decreased with SO₂ and NO_x emissions. Nevertheless, these emissions are still
576 relatively strong in the eastern USA (5 times higher than in the western USA) resulting in very acidic aerosols, with a pH
577 ranging from 2.2 in 1971 to 3.3 recently (Figs. 1 and S1). Such acidic conditions promote the dissolution of metals (e.g., Fe,
578 Mn, Cu) in ambient particles (Fang et al., 2017)(Fang et al., 2017). Soluble transition metals in atmospheric aerosols have
579 been linked to adverse health impacts since they generate reactive oxygen species, leading to oxidative stress and increased
580 toxicity of fine particulate matter (Fang et al., 2017;Park et al., 2018). Since the solubility of transition metals increases
581 exponentially below a pH of 3, the decrease of aerosol acidity over the eastern USA reported here suggests that the particles
582 have become substantially less toxic in the past few decades. Similar to Europe, the increasing pH has resulted in a growing
583 aerosol nitrate fraction from ~50% during the 1970s to 65% recently (Fig. 3), and to a strong increase of aerosol

584 hygroscopicity by ~0.15 units at the cloud base (Fig. 4). The role of NH₃ is critically important; without it the aerosol pH
585 over the eastern USA would be close to zero. Over the western USA, the aerosol pH is higher (~5), being affected by aeolian
586 dust from the Great Basin Desert, although NH₃ is still the most important alkaline buffer.

587 2.2.3 East and South Asia

588 In Asia, SO₂ and NO_x emissions have increased drastically since 1970. However, the simultaneous increase of NH₃
589 emissions along with the presence of mineral dust from the surrounding deserts (i.e., Gobi, Taklimakan, Thar) decelerated
590 the increase of aerosol acidity. Over East Asia, the aerosol pH decreased from about 5.3 during the 1970s to 4.5 in 2010.

591 This change in aerosol acidity has affected the predominant pathway of sulfate formation through ~~aqueous phase chemistry.~~
592 ~~Under acidic conditions, SO₂ is mainly oxidized by dissolved H₂O₂, while at pH > 5 the oxidation by O₃ predominates~~
593 ~~(Seinfeld and Pandis, 2006).~~ ~~aerosol aqueous phase chemistry. Under acidic conditions, SO₂ is mainly oxidized by transition~~
594 ~~metal ions, while at pH > 5 the oxidation by O₃ and NO₂ predominates (Cheng et al., 2016).~~ Therefore, the decrease of pH
595 during the last 50 years, even though being relatively modest, was sufficient to turn-off sulfate production from O₃ oxidation
596 (Fig. 5). At the same time, the increased aerosol acidity hinders the partitioning of nitric acid to the aerosol phase, reducing
597 the aerosol nitrate fraction from 90% to 80% (Fig. 3). Remarkably, the aerosol hygroscopicity has increased from ~0.3 in the
598 1970s to 0.45 recently (Fig. 4), revealing a reverse development compared to Europe and the USA. Here, the fraction of
599 mineral dust in the aerosol is higher; therefore, the particles gained hygroscopicity by the acquired pollution solutes.
600 Recently, the SO₂ emissions have dropped and the NO_x emission increase has slowed in East Asia, while SO₂ emissions are
601 soaring in South Asia. SO₂ emission trends since 2007 have been so drastic that inventories and scenarios tend to
602 ~~underestimate them overestimate the emitted SO₂.~~ Satellite observations indicate that India has recently overtaken China as
603 the world largest emitter of SO₂ (Li et al., 2017). Following the satellite observations, we implemented the ~~large significant~~
604 SO₂ ~~reduction~~ trends into our model (Fig. S2). Surprisingly, the effect only becomes noticeable over East Asia after 2016,
605 when the aerosol pH started increasing by about 0.3 units, while we do not find any change over South Asia. This
606 corroborates the strong buffering that we found over other regions such as Europe. Fig. 1 shows that NH₃ has been the major
607 buffer, supporting the recent findings of Zheng et al. (2020) that the acid-base pair of NH₄⁺/NH₃ provides the largest
608 buffering capacity over East and South Asia. However, we also found that in East Asia and to a lesser extent in South Asia
609 crustal elements, not considered in the study of Zheng et al. (2020), have contributed significantly on maintaining a mean pH
610 of 4.5 – 5 in the past decade (Fig. 1). ~~Calcium is the major crustal component of dust from the Gobi and Taklimakan deserts~~
611 ~~(Karydis et al., 2016) and unlike other crustal compounds it can react with sulfate ions and form insoluble CaSO₄, which~~
612 ~~precipitates out of the aerosol aqueous phase. This interaction reduces the aqueous sulfate and thus the aerosol acidity.~~

613 2.2.4 Tropical forests, Middle East

614 Over tropical forests, aerosols are typically not very acidic with pH values >4. Note that organic acids were not included in
615 the aerosol pH calculations, however, their contribution to the total ionic load is small (Andreae et al., 1988; Falkovich et al.,

616 2005), and aerosol acidity can be attributed to inorganic acids. Over the Amazon and Congo basins, the aerosol pH remained
617 around 5 since 1970. The Southeast Asian forest atmosphere is affected by pollution from mainland Asia, and the aerosol pH
618 decreased to around 4 recently. This pH drop has enhanced SOA formation from isoprene, since under low-NO_x conditions
619 (typical over rainforests) the presence of acidifying sulfate increases the reactive uptake of epoxydiols (Xu et al.,
620 2015;Surratt et al., 2010). Nevertheless, NH₃ emissions provide a remarkably strong buffer over all three tropical regions
621 while mineral dust cations are also important over the Amazon and Congo forests. Further, the Middle East is affected by
622 strong anthropogenic (fossil fuel related) and natural (aeolian dust) aerosol sources. Due to the high abundance of mineral
623 dust, the pH has remained close to 7. Without crustal cations, the pH would drop to about 4. Despite the omnipresence of
624 alkaline species from the surrounding deserts, NH₃ still plays a central role in controlling the acidification of mineral dust
625 aerosols, which can affect their hygroscopic growth and hence their climate forcing (Klingmuller et al., 2019;Klingmüller et
626 al., 2020).

627 2.2.5 Oceans

628 Over the Arctic and northern extra-tropical oceans, aerosol acidity is strongly affected by pollution transport from the
629 urban-industrial mid-latitudes. The Arctic aerosol pH is highly variable, remaining relatively low up to 1990 (~4.2), after
630 which it increased to about 5.2. Crustal cations are found to play a significant ~~buffering-role~~ lowering the aerosol acidity.
631 Over the northern extra-tropical oceans, aerosol pH has remained relatively constant (~4.8). NH₃ provides an important
632 alkaline buffer, and without it the aerosol pH would have been below 3. NH₃ is also proved to be important over the tropical
633 and southern extra-tropical oceans, where a noticeable increase in aerosol acidity occurred after June 1991, when the
634 eruption of Mount Pinatubo in the Philippines released ~20 million tons of SO₂ into the stratosphere (McCormick et al.,
635 1995). The impact of Pinatubo sulfate, after returning to the troposphere, on aerosol acidity is mostly evident over
636 Antarctica, where the pH dropped by 2 units, as the stratospheric circulation is strongest in the winter hemisphere. Over
637 Antarctica concentrations of dust and especially of NH₃ are very low, and Fig. 1 illustrates that only in this pristine
638 environment the large Pinatubo anomaly could overwhelm the buffering by alkaline species. Except after Pinatubo, the pH
639 has remained nearly constant at 5.8 over Antarctica and about 5.5 in the tropics and 6.8 in the southern extra-tropics.

640 3. Conclusions

641 We find that aerosol pH is generally well-buffered by alkaline compounds, notably NH₃ and in some areas crustal
642 elements. NH₃ is found to supply remarkable buffering capacity on a global scale, from the polluted continents to the remote
643 oceans. In the absence of NH₃, aerosols would be highly (to extremely) acidic in most of the world. Therefore, potential
644 future changes in NH₃ are critically important in this respect. Agriculture is the main NH₃ source and a controlling factor in
645 fine particle concentrations and health impacts in some areas (e.g., Europe) (Pozzer et al., 2017). The control of agricultural
646 ammonia emissions must therefore be accompanied by very strong reductions of SO₂ and NO_x to avoid that aerosols become
647 highly acidic with implications for human health (aerosol toxicity), ecosystems (acid deposition and nutrient availability),
648 clouds and climate (aerosol hygroscopicity).

649 4. Appendix A: Materials and Methods

650 4.1 Aerosol-chemistry-climate model

651 We used the ECHAM5/MESSy Atmospheric Chemistry (EMAC) model, which is a numerical chemistry and climate
652 simulation system that describes lower and middle atmosphere processes (Jöckel et al., 2006). EMAC uses the
653 Modular Earth Submodel System (MESSy2) (Jöckel et al., 2010) to link the different sub-models with an atmospheric
654 dynamical core, being an updated version of the 5th generation European Centre - Hamburg general circulation
655 model (ECHAM5) (Roeckner et al., 2006). EMAC has been extensively described and evaluated against in situ
656 observations and satellite retrievals to compute particulate matter concentrations and composition, aerosol optical
657 depth, acid deposition, gas phase mixing ratios, cloud properties, and meteorological parameters (Karydis et al.,
658 2016; Pozzer et al., 2012; Tsimpidi et al., 2016; Karydis et al., 2017; Bacer et al., 2018). The spectral resolution of EMAC
659 used in this study is T63L31, corresponding to a horizontal grid resolution of approximately $1.9^\circ \times 1.9^\circ$ and 31 vertical
660 layers extending up to 10 hPa (i.e., 25 km) from the surface. The presented model simulations encompass the 50-year
661 period 1970-2020.

662 EMAC calculates fields of gas phase species online through the Module Efficiently Calculating the Chemistry of the
663 Atmosphere (MECCA) Submodel (Sander et al., 2019). MECCA calculates the concentration of a range of gases,
664 including aerosol precursor species (e.g. SO_2 , NH_3 , NO_x , DMS, H_2SO_4 and DMSO) and the major oxidant species (e.g.
665 OH, H_2O_2 , NO_3 , and O_3). Aerosol microphysics are calculated by the Global Modal-aerosol eXtension (GMXe) module
666 (Pringle et al., 2010). The organic aerosol formation and atmospheric evolution are calculated by the ORACLE
667 Submodel (Tsimpidi et al., 2014, 2018). The aerosol size distribution is described by seven lognormal modes: four
668 hydrophilic modes that cover the aerosol size spectrum of nucleation, Aitken, accumulation and coarse modes, and
669 three hydrophobic modes that cover the same size range except nucleation. The aerosol composition within each size
670 mode is uniform (internally mixed), however, it varies between modes (externally mixed). Each mode is defined in
671 terms of total number concentration, number mean radius, and geometric standard deviation (Pringle et al., 2010).
672 The removal of gas and aerosol species through wet and dry deposition is calculated within the SCAV (Tost et al.,
673 2006) and DRYDEP (Kerkweg et al., 2006) submodels, respectively. The sedimentation of aerosols is calculated
674 within the SEDI submodel (Kerkweg et al., 2006). The cloud cover, microphysics and precipitation of large scale
675 clouds is calculated by the CLOUD Submodel (Roeckner et al., 2006) which uses a two-moment stratiform
676 microphysical scheme (Lohmann and Ferrachat, 2010), and describes liquid droplet (Karydis et al., 2017) and ice
677 crystal (Bacer et al., 2018) formation by accounting for the aerosol physicochemical properties. The effective
678 hygroscopicity parameter κ is used to describe the influence of chemical composition on the cloud condensation
679 nuclei (CCN) activity of atmospheric aerosols. κ is calculated using the mixing rule of Petters and Kreidenweis
680 (Petters and Kreidenweis, 2007) and the individual κ parameter values for each inorganic salt (Petters and
681 Kreidenweis, 2007; Sullivan et al., 2009). Organic aerosol species are assumed to have a constant hygroscopicity
682 κ parameter κ of 0.14 while bulk mineral dust and black carbon are assumed to have zero hygroscopicity.

683 4.2 Emissions

684 The vertically distributed (Pozzer et al., 2009) CMIP5 RCP8.5 emission inventory (van Vuuren et al., 2011) is used for
685 the anthropogenic and biomass burning emissions during the years 1970-2020. Direct emissions of aerosol
686 components from biofuel and open biomass burning are considered by using scaling factors applied on the emitted
687 black carbon based on the findings of Akagi et al. (Akagi et al., 2011) (Table S2). Dust emission fluxes and emissions of
688 crustal species (Ca^{2+} , Mg^{2+} , K^+ , Na^+) are calculated online as described by Klingmüller, et al. (Klingmüller et al., 2018)
689 and based on the chemical composition of the emitted soil particles in every grid cell (Karydis et al., 2016); Table S3.

690 NO_x produced by lightning is calculated online and distributed vertically based on the parameterization of Grewe, et
691 al. (Grewe et al., 2001). The emissions of NO from soils are calculated online based on the algorithm of Yienger and
692 Levy (Yienger and Levy, 1995). The oceanic DMS emissions are calculated online by the AIRSEA Submodel (Pozzer et
693 al., 2006). The natural emissions of NH₃ are based on the GEIA database (Bouwman et al., 1997). Emissions of sea
694 spray aerosols (assuming a composition suggested by Seinfeld and Pandis (Seinfeld and Pandis, 2006); Table S2) and
695 volcanic degassing emissions of SO₂ are based on the offline emission data set of AEROCOM (Dentener et al., 2006).

697 **4.3 Thermodynamic model**

698 The inorganic aerosol composition, which is of prime importance for the accurate pH calculation, is computed with
699 the ISORROPIA-II thermodynamic equilibrium model (Fountoukis and Nenes, 2007). ISORROPIA-II calculates the
700 gas/liquid/solid equilibrium partitioning of the K⁺-Ca²⁺-Mg²⁺-NH₄⁺-Na⁺-SO₄²⁻-NO₃⁻-Cl-H₂O aerosol system and
701 considers the presence of 15 aqueous phase components and 19 salts in the solid phase. ISORROPIA-II solves for the
702 equilibrium state by considering the chemical potential of the species and minimizes the number of equations and
703 iterations required by considering specific compositional “regimes”. ~~Furthermore, to~~ The assumption of
704 thermodynamic equilibrium is a good approximation for fine-mode aerosols that rapidly reach equilibrium. However,
705 the equilibrium timescale for large particles is typically larger than the time step of the model (Meng and Seinfeld,
706 1996) leading to errors in the size distribution of semi-volatile ions like nitrate. Since the current study include
707 reactions of nitric acid with coarse sea-salt and dust aerosol cations, the competition of fine and coarse particles for
708 the available nitric acid can only be accurately represented by taking into account the kinetic limitations during
709 condensation of HNO₃ in the coarse mode aerosols. To account for kinetic limitations by mass transfer and transport
710 between the gas and particle phases, the process of gas/aerosol partitioning is calculated in two stages (Pringle et al.,
711 2010). First, the gaseous species that kinetically condense onto the aerosol phase within the model timestep are
712 calculated assuming diffusion limited condensation (Vignati et al., 2004). Then, ISORROPIA-II re-distributes the mass
713 between the gas and the aerosol phase assuming instant equilibrium between the two phases.

714 ISORROPIA-II is used in the forward mode, in which the total (i.e., gas and aerosol) concentrations are given as
715 input. Reverse mode calculations (i.e. when only the aerosol phase composition is known) should be avoided since
716 they are sensitive to errors and infer bimodal ~~behavior~~ behaviour with highly acidic or highly alkaline particles,
717 depending on whether anions or cations are in excess (Song et al., 2018). While it is often assumed that aerosols are
718 in a metastable state (i.e., composed only of a supersaturated aqueous phase), here we use ISORROPIA-II in the
719 thermodynamically stable state mode where salts are allowed to precipitate once the aqueous phase becomes
720 saturated. For this purpose, we have used the revised ISORROPIA-II model which includes modifications proposed by
721 Song et al. (2018), who resolved coding errors related to pH calculations when the stable state assumption is used. A
722 sensitivity simulation with only liquid aerosols (i.e., metastable) revealed that the assumed particle phase state does
723 not significantly impact the pH calculations over oceans and polluted regions (e.g., Europe), however, the metastable
724 assumption produces more acidic particles (up to 2 units of pH) in regions affected by high concentrations of crustal
725 cations (Fig. S3). Overall, the stable state assumption used here produces about 0.5 units higher global average pH
726 than the metastable assumption. By comparing with the benchmark thermodynamic model E-AIM, Song et al. (2018)
727 found that ISORROPIA-II produces somewhat higher pH (by 0.1-0.7 units, negatively correlated with RH). However,
728 E-AIM model versions either lack crustal cations from the ambient mixture of components (e.g. version II) (Clegg et
729 al., 1998), or only include Na⁺ with the restriction that it should be used when RH> 60% (e.g. version IV) (Frieze and
730 Ebel, 2010). Song et al. (2018) applied the revised ISORROPIA-II during winter haze events in eastern China and
731 found that the assumed particle phase state, either stable or metastable, does not significantly impact the pH
732 predictions.

We performed a sensitivity simulation with only liquid aerosols (i.e., metastable), which revealed that the assumed particle phase state does not significantly impact the pH calculations over oceans and polluted regions (e.g., Europe), however, the metastable assumption produces more acidic particles (up to 2 units of pH) in regions affected by high concentrations of crustal cations and consistently low RH values (Fig. S3). Fountoukis et al. (2007) have shown that the metastable solution predicts significant amounts of water below the mutual deliquescence relative humidity (MDRH, where all salts are simultaneously saturated with respect to all components). Further, the generally high calcium concentrations downwind of deserts results in increasing pH values due to the precipitation of insoluble salts such as the CaSO_4 . The metastable state assumption fails to reproduce this since it treats only the ions in the aqueous phase. In general, high amounts of crustal species can significantly increase the aerosol pH which is consistent with the presence of excess carbonate in the aerosol phase (Meng et al., 1995). It is worth mentioning that the stable state solution algorithm of ISORROPIA II starts with assuming a dry aerosol, and based on the ambient RH dissolves each of the salts depending on their DRH. However, in the ambient atmosphere, when the RH over a wet particle is decreasing, the wet aerosol may not crystallize below the MDRH but instead remain in a metastable state affecting the uptake of water by the aerosol and thus the pH. This could be the case in some locations with high diurnal variations of RH. Our sensitivity calculations show that, overall, the stable state assumption produces an about 0.5 units higher global average pH than the metastable assumption. Karydis et al. (2016) have shown that while the aerosol state assumption has a marginal effect on the calculated nitrate aerosol tropospheric burden (2% change), it can be important over and downwind of deserts at very low RHs where nitrate is reduced by up to 60% by using the metastable assumption. This is in accord with the findings of Ansari and Pandis (2000) who suggested that the stable state results in higher concentrations of aerosol nitrate when the RH is low (<35 %) and/or sulfate to nitrate molar ratios are low (<0.25).

4.4 pH calculations

The pH is defined as the negative decimal logarithm of the hydrogen ion activity ($a_{\text{H}^+} = \gamma x_{\text{H}^+}$) in a solution:

$$pH = -\log_{10}(\gamma x_{\text{H}^+}),$$

$$pH = -\log_{10}(\gamma x_{\text{H}^+}) \quad (A1)$$

where x_{H^+} is the molality of hydrogen ions in the solution and γ is the ion activity coefficient of hydrogen.

Assuming that γ is unity, the aerosol pH can be calculated by using the hydrogen ion concentration in the aqueous aerosol phase calculated by ISORROPIA-II (in mole m^{-3}) and the aerosol water content calculated by GMXe (in mole Kg^{-1}). GMXe assumes that particle modes are internally mixed, and takes into account the contribution of both inorganic and organic (based on the organic hygroscopicity parameter, $\kappa_{\text{org}} = 0.14$) species to aerosol water.

The aerosol pH is calculated online at each timestep, and output stored every five hours based on instantaneous concentrations of fine aerosol water and hydrogen ions. The average pH values shown in the manuscript are based on the calculated instantaneous mean pH values. According to the Jensen's inequality (Jensen, 1906), the average of the instantaneous pH values is less than or equal to the pH calculated based on the average of the water and hydrogen ion instantaneous values. We estimate that the average pH calculated based on 5-hourly instantaneous values is approximately 1-3 (~2 globally averaged) units higher than the pH calculated based on the average water and hydrogen ion concentrations. By including online gas-particle partitioning calculations of the NH_3/HNO_3 system in polluted air, as applied here, we find that the aerosol pH is higher by approximately one unit (Guo et al., 2015). Hence by neglecting these aspects the aerosol pH would be low-biased by about 3 points.

4.5 Comparison against pH estimations from field derived PM_{2.5} compositional data

The pH calculated here is compared against pH estimations from field derived PM_{2.5} compositional data around the world compiled by Pye et al. (2020) (Table S1). pH data derived from other aerosol sizes (e.g., PM₁) has been omitted since aerosol acidity can vary significantly with size (Zakoura et al., 2020). It should be emphasized that the comparison presented in Table S1 aims to corroborate the spatial variability of pH found in this study and not to strictly evaluate the model calculations. Observationally estimated aerosol pH is derived from a variety of methods that can affect the result significantly as discussed above (i.e., the use of E-AIM or ISORROPIA, stable/metastable assumption, forward/reverse mode, and the availability of gas phase NH₃/HNO₃, crustal species, and organic aerosol water observations).—evaluate the model calculations. Since direct measurements of aerosol acidity are not available, the observation-based aerosol pH is estimated by employing thermodynamic equilibrium models (e.g., ISORROPIA) and making assumptions that can significantly affect the results, especially when the data are averaged over extended periods, while RH conditions during data collection are not always accounted for, e.g. in studies based on filter sampling. The calculation of aerosol acidity on a global scale requires the advanced treatment of atmospheric aerosol chemical complexity, representing the real atmosphere, and beyond the conventional methods used by chemistry-climate models (CCM). The atmospheric chemistry model system EMAC is an ideal tool for this purpose since it is one of the most comprehensive CCM containing advanced descriptions of the aerosol thermodynamics (including e.g. dust-pollution interactions) and organic aerosol formation and atmospheric aging (affecting the aerosol water). Our model calculations for aerosol acidity are based on some processes/factors that are not included explicitly, usually neglected by model calculations used to constrain the aerosol acidity from observations. Sources of discrepancy between the pH calculations can be the following:

- 4.4 The stable/metastable assumption does not affect the pH most of the time, however, in some cases with low RHs and the presence of crustal cations, the metastable assumption results in lower pHs (see section 4.3).
- Crustal species from deserts and Na⁺ from sea salt can elevate the pH significantly in some locations, however, these are often neglected in observations.
- The organic aerosols (which are treated comprehensively by our model using the module ORACLE and the volatility basis set framework (Tsimpidi et al., 2014)) can contribute significantly to the aerosol water, and thus increase the aerosol pH. This contribution is not considered by many observational studies.
- Including gas phase species (e.g., NH₃, HNO₃) in the pH calculations is important. Using only the aerosol-phase as input (i.e., reverse mode) the inferred pH exhibits bimodal behaviour with very acidic or alkaline values depending on whether anions or cations are in excess (Hennigan et al., 2015). Even if the forward mode is used (without gas phase input), the calculated aerosol pH is biased low (approximately 1 pH unit) due to the repartition of semi-volatile anions (i.e., NH₃) to the gas phase to establish equilibrium (Guo et al., 2015).
- Another important aspect, not explicitly mentioned in many studies, relates to the methods used to derive the campaign-average (or for 3D models the simulated average) pH. In our model the aerosol pH is calculated online (2-minute time resolution), while output is stored every five hours based on instantaneous concentrations of fine aerosol H₂O and H⁺. This mimics 5-hourly aerosol sampling. Then, the average pH values are calculated from the instantaneous mean pH values (see section 4.4). Often models use average values (and not instantaneous) as

810 output, or field-derived pH calculations use average observed H₂O and H⁺ values, which can result in important
811 underestimation (by ~ 1-3 units) of the aerosol pH (Jensen, 1906).

812 • Some unrealistically high pH values in a few past studies resulted from coding errors in the stable state
813 assumption of the ISORROPIA II model, which have been corrected in our study following the recommendation
814 of Song et al. (2018).

815 • The type of thermodynamic model used is also important. Song et al. (2018) found that ISORROPIA-II produces
816 somewhat higher pH (by 0.1-0.7 units, negatively correlated with RH) compared to the thermodynamic model E-
817 AIM, which is used to observationally-constrain pH in some studies.

818 • Measurements of PM_{2.5} nitrate are not always reliable because of artifacts associated with the volatility of
819 ammonium nitrate (Schaap et al., 2004). Ammonium and nitrate can partially evaporate from Teflon filters at
820 temperatures between 15 to 20 °C and can evaporate completely at temperatures above. The evaporation from
821 quartz filters is also significant at temperatures higher than 20 °C. This systematic underestimation of
822 ammonium nitrate can affect the observed chemical composition of the aerosol and thus the pH calculations.

823 • The comparison between global model output and observations at specific locations. This also concerns the
824 aerosol concentrations but is especially important for the aerosol acidity. Apart from the size of the model grid
825 cells (i.e., ~ 1.9°x1.9°), the altitude is also important. The first vertical layer of EMAC is approximately 67m in
826 height. On the other hand, ground observations are typically collected in a height up to 3 m. While the aerosols
827 within size modes simulated in our model are well-mixed, perhaps this is not the case for the aerosols observed
828 at the surface and potentially close to sources, and thus the aerosol acidity may be higher (e.g., due to the higher
829 contribution from local primary sources like SO₄²⁻, lower water amounts in the aerosol, or lower concentrations
830 of semi-volatile cations like NH₄⁺).

832 4.6 Emissions

833 The vertically distributed (Pozzer et al., 2009) CMIP5 RCP8.5 emission inventory (van Vuuren et al., 2011) is used for
834 the anthropogenic and biomass burning emissions during the years 1970-2020. Direct emissions of aerosol
835 components from biofuel and open biomass burning are considered by using scaling factors applied on the emitted
836 black carbon based on the findings of Akagi, et al. (Akagi et al., 2011) (Table S2). Dust emission fluxes and emissions
837 of crustal species (Ca²⁺, Mg²⁺, K⁺, Na⁺) are calculated online as described by Klingmuller, et al. (Klingmuller et al.,
838 2018) and based on the chemical composition of the emitted soil particles in every grid cell (Karydis et al., 2016),
839 Table S3. NO_x produced by lightning is calculated online and distributed vertically based on the parameterization of
840 Grewe, et al. (Grewe et al., 2001). The emissions of NO from soils are calculated online based on the algorithm of
841 Yienger and Levy (Yienger and Levy, 1995). The oceanic DMS emissions are calculated online by the AIRSEA

842 Submodel (Pozzer et al., 2006). The natural emissions of NH₃ are based on the GEIA database (Bouwman et al., 1997).
 843 Emissions of sea spray aerosols (assuming a composition suggested by Seinfeld and Pandis (Seinfeld and Pandis,
 844 2006), Table S2) and volcanic degassing emissions of SO₂ are based on the offline emission data set of AEROCOM
 845 (Dentener et al., 2006).

846 4.5 Partitioning of nitric acid between the gas and aerosol phases

847 The impact of pH on the fraction of nitrate in the particle phase relative to total nitrate (gas plus particle), i.e.,
 848 $\varepsilon(\text{NO}_3^-)$, during the 50 years of simulation in specific regions is calculated as follows (Nah et al., 2018):

$$849 \quad \varepsilon(\text{NO}_3^-) = \frac{H_{\text{HNO}_3}^* WRT(0.987 \times 10^{-14})}{\gamma_{\text{NO}_3^-} \gamma_{\text{H}^+} 10^{-\text{pH}} + H_{\text{HNO}_3}^* WRT(0.987 \times 10^{-14})} \quad (A2)$$

850 Where $H_{\text{HNO}_3}^*$ is the combined molality-based equilibrium constant of HNO₃ dissolution and deprotonation, γ 's
 851 represent the activity coefficients, W is the aerosol water, R is the gas constant, and T is the ambient temperature. Eq.
 852 A2 is equivalent with the instantaneous calculations of ISOROPIA II within EMAC. However, the model output is
 853 produced after considering all processes in the model and is not calculated at every timestep. Therefore, the use of
 854 Eq. 2 can provide a clearer picture of the impact of pH on HNO₃ gas/particle partitioning since the model output (e.g.,
 855 gas-phase HNO₃ and nitrate in 4 size modes) is subject to uncertainties related to other processes (e.g., deposition,
 856 coagulation, transport, etc.).

Formatted: Font: Times

857 4.6.7 Sulfate formation in aqueous aerosols

858 The sulfate production rate on aqueous aerosols from the heterogeneous oxidation of S(IV) with the dissolved O₃ is
 859 given by

$$860 \quad R_{\text{O}} = k [\text{O}_3] \quad (A3)$$

861 The first-order uptake rate, k , from monodisperse aerosols with radius r_a and total aerosol surface A , is calculated
 862 following Jacob (Jacob, 2000):

$$864 \quad k = \left(\frac{\gamma_{\alpha}}{D_g} + \frac{4}{v\gamma} \right)^{-1} A \quad (A4)$$

865 where v is the mean molecular speed of O₃ and D_g is its gas-phase molecular diffusion coefficient calculated as
 866 follows:

$$867 \quad D_g = \frac{9.45 \times 10^{17} \times \sqrt{T \left(3.47 \times 10^{-2} + \frac{1}{M} \right)}}{\rho_{\text{air}}} \quad (A5)$$

868 where T is the ambient air temperature, ρ_{air} is the air density, and M the molar mass of O₃. γ is the reaction
 869 probability calculated following Jacob (Jacob, 2000) and Shao et al. (Shao et al., 2019).

$$870 \quad \gamma = \left(\frac{1}{\alpha} + \frac{v}{4HRT \sqrt{D_{\alpha} K f_r}} \right)^{-1} \quad (A6)$$

871 where α is the mass accommodation coefficient, D_{α} is the aqueous-phase molecular diffusion coefficient of O₃, H is the
 872 effective Henry's law constant of O₃ (Sander, 2015), R is the ideal gas constant, f_r is the reacto-diffusive correction term
 873 (Shao et al., 2019), and K is the pseudo-first order reaction rate constant between S(IV) and O₃ in the aqueous phase
 874 (Seinfeld and Pandis, 2006).
 875

Formatted: Font: Cambria Math

876 **5. References**

- 877 [Abdelkader, M., Metzger, S., Mamouri, R. E., Astitha, M., Barrie, L., Levin, Z., and Lelieveld, J.: Dust-air pollution dynamics](#)
878 [over the eastern Mediterranean, Atmospheric Chemistry and Physics, 15, 9173-9189, 10.5194/acp-15-9173-2015, 2015.](#)
- 879 [Akagi, S. K., Yokelson, R. J., Wiedinmyer, C., Alvarado, M. J., Reid, J. S., Karl, T., Crounse, J. D., and Wennberg, P. O.:](#)
880 [Emission factors for open and domestic biomass burning for use in atmospheric models, Atmospheric Chemistry and](#)
881 [Physics, 11, 4039-4072, 10.5194/acp-11-4039-2011, 2011.](#)
- 882 [Andreae, M. O., Talbot, R. W., Andreae, T. W., and Harriss, R. C.: Formic and acetic acid over the central Amazon region,](#)
883 [Brazil. 1. dry season, Journal of Geophysical Research-Atmospheres, 93, 1616-1624, 10.1029/JD093iD02p01616, 1988.](#)
- 884 [Ansari, A. S., and Pandis, S. N.: The effect of metastable equilibrium states on the partitioning of nitrate between the gas](#)
885 [and aerosol phases, Atmospheric Environment, 34, 157-168, 10.1016/s1352-2310\(99\)00242-3, 2000.](#)
- 886 [Bacer, S., Sullivan, S. C., Karydis, V. A., Barahona, D., Kramer, M., Nenes, A., Tost, H., Tsimpidi, A. P., Lelieveld, J., and](#)
887 [Poizzer, A.: Implementation of a comprehensive ice crystal formation parameterization for cirrus and mixed-phase](#)
888 [clouds in the EMAC model \(based on MESSy 2.53\), Geoscientific Model Development, 11, 4021-4041, 10.5194/gmd-11-](#)
889 [4021-2018, 2018.](#)
- 890 [Behera, S. N., Betha, R., Liu, P., and Balasubramanian, R.: A study of diurnal variations of PM2.5 acidity and related](#)
891 [chemical species using a new thermodynamic equilibrium model, Science of The Total Environment, 452-453, 286-295,](#)
892 [https://doi.org/10.1016/j.scitotenv.2013.02.062, 2013.](#)
- 893 [Bouwman, A. F., Lee, D. S., Asman, W. A. H., Dentener, F. J., VanderHoek, K. W., and Olivier, J. G. J.: A global high-resolution](#)
894 [emission inventory for ammonia, Global Biogeochemical Cycles, 11, 561-587, 10.1029/97gb02266, 1997.](#)
- 895 [Cheng, Y. F., Zheng, G. J., Wei, C., Mu, Q., Zheng, B., Wang, Z. B., Gao, M., Zhang, Q., He, K. B., Carmichael, G., Poschl, U.,](#)
896 [and Su, H.: Reactive nitrogen chemistry in aerosol water as a source of sulfate during haze events in China, Science](#)
897 [Advances, 2, 10.1126/sciadv.1601530, 2016.](#)
- 898 [Clegg, S. L., Brimblecombe, P., and Wexler, A. S.: Thermodynamic model of the system H+-NH4+-Na+-SO42--NB3--Cl--H2O](#)
899 [at 298.15 K, J. Phys. Chem. A, 102, 2155-2171, 10.1021/jp973043j, 1998.](#)
- 900 [Dall'Osto, M., Airs, R. L., Beale, R., Cree, C., Fitzsimons, M. F., Beddows, D., Harrison, R. M., Ceburnis, D., O'Dowd, C.,](#)
901 [Rinaldi, M., Paglione, M., Nenes, A., Decesari, S., and Simó, R.: Simultaneous Detection of Alkylamines in the Surface](#)
902 [Ocean and Atmosphere of the Antarctic Sympagic Environment, ACS Earth and Space Chemistry, 3, 854-862,](#)
903 [10.1021/acsearthspacechem.9b00028, 2019.](#)
- 904 [Dentener, F., Kinne, S., Bond, T., Boucher, O., Cofala, J., Generoso, S., Ginoux, P., Gong, S., Hoelzemann, J. J., Ito, A., Marelli,](#)
905 [L., Penner, J. E., Putaud, J. P., Textor, C., Schulz, M., van der Werf, G. R., and Wilson, J.: Emissions of primary aerosol and](#)
906 [precursor gases in the years 2000 and 1750 prescribed data-sets for AeroCom, Atmos. Chem. Phys., 6, 4321-4344, 2006.](#)
- 907 [Falkovich, A. H., Graber, E. R., Schkolnik, G., Rudich, Y., Maenhaut, W., and Artaxo, P.: Low molecular weight organic acids](#)
908 [in aerosol particles from Rondonia, Brazil, during the biomass-burning, transition and wet periods, Atmospheric](#)
909 [Chemistry and Physics, 5, 781-797, 10.5194/acp-5-781-2005, 2005.](#)
- 910 [Fang, T., Guo, H. Y., Zeng, L. H., Verma, V., Nenes, A., and Weber, R. J.: Highly Acidic Ambient Particles, Soluble Metals, and](#)
911 [Oxidative Potential: A Link between Sulfate and Aerosol Toxicity, Environmental Science & Technology, 51, 2611-2620,](#)
912 [10.1021/acs.est.6b06151, 2017.](#)
- 913 [Fountoukis, C., and Nenes, A.: ISORROPIA II: a computationally efficient thermodynamic equilibrium model for K+-Ca2+-](#)
914 [Mg2+-NH4+-Na+-SO42--NO3--Cl--H2O aerosols, Atmospheric Chemistry and Physics, 7, 4639-4659, 2007.](#)
- 915 [Friese, E., and Ebel, A.: Temperature Dependent Thermodynamic Model of the System](#)
916 [H+-NH4+-Na+-SO42--NO3--Cl--H2O, The Journal of Physical Chemistry A, 114, 11595-11631, 10.1021/jp101041j,](#)
917 [2010.](#)
- 918 [Grewé, V., Brunner, D., Dameris, M., Grenfell, J. L., Hein, R., Shindell, D., and Staehelin, J.: Origin and variability of upper](#)
919 [tropospheric nitrogen oxides and ozone at northern mid-latitudes, Atmospheric Environment, 35, 3421-3433,](#)
920 [10.1016/s1352-2310\(01\)00134-0, 2001.](#)

Formatted: Font: +Body (Calibri), 10 pt, English (United States)

Formatted: Indent: Left: 0 cm, Hanging: 0.5 cm

Formatted: Font: +Body (Calibri), 10 pt, English (United States)

Formatted: Indent: Left: 0 cm, Hanging: 0.5 cm

Formatted: Font: +Body (Calibri), 10 pt, English (United States)

921 Guo, H., Xu, L., Bougiatioti, A., Cerully, K. M., Capps, S. L., Hite, J. R., Carlton, A. G., Lee, S. H., Bergin, M. H., Ng, N. L., Nenes,
922 A., and Weber, R. J.: Fine-particle water and pH in the southeastern United States, *Atmospheric Chemistry and Physics*,
923 15, 5211-5228, 10.5194/acp-15-5211-2015, 2015.

924 Guo, H., Sullivan, A. P., Campuzano-Jost, P., Schroder, J. C., Lopez-Hilfiker, F. D., Dibb, J. E., Jimenez, J. L., Thornton, J. A.,
925 Brown, S. S., Nenes, A., and Weber, R. J.: Fine particle pH and the partitioning of nitric acid during winter in the
926 northeastern United States, *Journal of Geophysical Research-Atmospheres*, 121, 10355-10376, 10.1002/2016jd025311,
927 2016.

928 Guo, H., Otjes, R., Schlag, P., Kiendler-Scharr, A., Nenes, A., and Weber, R. J.: Effectiveness of ammonia reduction on
929 control of fine particle nitrate, *Atmospheric Chemistry and Physics*, 18, 12241-12256, 10.5194/acp-18-12241-2018,
930 2018.

931 Guo, H. Y., Liu, J. M., Froyd, K. D., Roberts, J. M., Veres, P. R., Hayes, P. L., Jimenez, J. L., Nenes, A., and Weber, R. J.: Fine
932 particle pH and gas-particle phase partitioning of inorganic species in Pasadena, California, during the 2010 CalNex
933 campaign, *Atmospheric Chemistry and Physics*, 17, 5703-5719, 10.5194/acp-17-5703-2017, 2017.

934 Hennigan, C. J., Izumi, J., Sullivan, A. P., Weber, R. J., and Nenes, A.: A critical evaluation of proxy methods used to estimate
935 the acidity of atmospheric particles, *Atmospheric Chemistry and Physics*, 15, 2775-2790, 10.5194/acp-15-2775-2015,
936 2015.

937 Jacob, D. J.: Heterogeneous chemistry and tropospheric ozone, *Atmospheric Environment*, 34, 2131-2159, 10.1016/s1352-
938 2310(99)00462-8, 2000.

939 Jensen, J.: On the convex functions and inequalities between mean values, *Acta Mathematica*, 30, 175-193,
940 10.1007/bf02418571, 1906.

941 Jia, S., Wang, X., Zhang, Q., Sarkar, S., Wu, L., Huang, M., Zhang, J., and Yang, L.: Technical note: Comparison and
942 interconversion of pH based on different standard states for aerosol acidity characterization, *Atmos. Chem. Phys.*, 18,
943 11125-11133, 10.5194/acp-18-11125-2018, 2018.

944 Jickells, T. D., An, Z. S., Andersen, K. K., Baker, A. R., Bergametti, G., Brooks, N., Cao, J. J., Boyd, P. W., Duce, R. A., Hunter, K.
945 A., Kawahata, H., Kubilay, N., IlaRoche, J., Liss, P. S., Mahowald, N., Prospero, J. M., Ridgwell, A. J., Tegen, I., and Torres,
946 R.: Global iron connections between desert dust, ocean biogeochemistry, and climate, *Science*, 308, 67-71,
947 10.1126/science.1105959, 2005.

948 Jöckel, P., Tost, H., Pozzer, A., Bruehl, C., Buchholz, J., Ganzeveld, L., Hoor, P., Kerkweg, A., Lawrence, M. G., Sander, R.,
949 Steil, B., Stiller, G., Tanarhte, M., Taraborrelli, D., Van Aardenne, J., and Lelieveld, J.: The atmospheric chemistry general
950 circulation model ECHAM5/MESSy1: consistent simulation of ozone from the surface to the mesosphere, *Atmos. Chem.*
951 *Phys.*, 6, 5067-5104, 2006.

952 Jöckel, P., Kerkweg, A., Pozzer, A., Sander, R., Tost, H., Riede, H., Baumgaertner, A., Gromov, S., and Kern, B.: Development
953 cycle 2 of the Modular Earth Submodel System (MESSy2), *Geoscientific Model Development*, 3, 717-752, 2010.

954 Karydis, V. A., Tsimpidi, A. P., Pozzer, A., Astitha, M., and Lelieveld, J.: Effects of mineral dust on global atmospheric nitrate
955 concentrations, *Atmos. Chem. Phys.*, 16, 1491-1509, 10.5194/acp-16-1491-2016, 2016.

956 Karydis, V. A., Tsimpidi, A. P., Bacer, S., Pozzer, A., Nenes, A., and Lelieveld, J.: Global impact of mineral dust on cloud
957 droplet number concentration, *Atmospheric Chemistry and Physics*, 17, 5601-5621, 10.5194/acp-17-5601-2017, 2017.

958 Kerkweg, A., Buchholz, J., Ganzeveld, L., Pozzer, A., Tost, H., and Jöckel, P.: Technical Note: An implementation of the dry
959 removal processes DRY DEPosition and SEDimentation in the Modular Earth Submodel System (MESSy), *Atmos. Chem.*
960 *Phys.*, 6, 4617-4632, 2006.

961 Klingmüller, K., Metzger, S., Abdelkader, M., Karydis, V. A., Stenchikov, G. L., Pozzer, A., and Lelieveld, J.: Revised mineral
962 dust emissions in the atmospheric chemistry-climate model EMAC (MESSy 2.52 DU_Astitha1 KKDU2017 patch),
963 *Geoscientific Model Development*, 11, 989-1008, 10.5194/gmd-11-989-2018, 2018.

964 Klingmüller, K., Lelieveld, J., Karydis, V. A., and Stenchikov, G. L.: Direct radiative effect of dust-pollution interactions,
965 *Atmospheric Chemistry and Physics*, 19, 7397-7408, 10.5194/acp-19-7397-2019, 2019.

966 Klingmüller, K., Karydis, V. A., Bacer, S., Stenchikov, G. L., and Lelieveld, J.: Weaker cooling by aerosols due to dust-pollution
967 interactions, *Atmos. Chem. Phys. Discuss.*, 2020, 1-19, 10.5194/acp-2020-531, 2020.

968 Lawal, A. S., Guan, X. B., Liu, C., Henneman, L. R. F., Vasilakos, P., Bhogineni, V., Weber, R. J., Nenes, A., and Russell, A. G.:
 969 Linked Response of Aerosol Acidity and Ammonia to SO₂ and NO_x Emissions Reductions in the United States,
 970 Environmental Science & Technology, 52, 9861-9873, 10.1021/acs.est.8b00711, 2018.

971 Lelieveld, J., Evans, J. S., Fnais, M., Giannadaki, D., and Pozzer, A.: The contribution of outdoor air pollution sources to
 972 premature mortality on a global scale, Nature, 525, 367-371, 10.1038/nature15371, 2015.

973 Leygraf, C., Wallinder, I. O., Tidblad, J., and Graedel, T.: Atmospheric Corrosion, John Wiley & Sons, 2016.

974 Li, C., McLinden, C., Fioletov, V., Krotkov, N., Carn, S., Joiner, J., Streets, D., He, H., Ren, X., Li, Z., and Dickerson, R. R.: India
 975 is Overtaking China as the World's Largest Emitter of Anthropogenic Sulfur Dioxide, Scientific Reports, 7, 14304,
 976 10.1038/s41598-017-14639-8, 2017.

977 Lohmann, U., and Ferrachat, S.: Impact of parametric uncertainties on the present-day climate and on the anthropogenic
 978 aerosol effect, Atmos. Chem. Phys., 10, 11373-11383, 10.5194/acp-10-11373-2010, 2010.

979 Marais, E. A., Jacob, D. J., Jimenez, J. L., Campuzano-Jost, P., Day, D. A., Hu, W., Krechmer, J., Zhu, L., Kim, P. S., Miller, C. C.,
 980 Fisher, J. A., Travis, K., Yu, K., Hanisco, T. F., Wolfe, G. M., Arkinson, H. L., Pye, H. O. T., Froyd, K. D., Liao, J., and McNeill,
 981 V. F.: Aqueous-phase mechanism for secondary organic aerosol formation from isoprene: application to the southeast
 982 United States and co-benefit of SO₂ emission controls, Atmospheric Chemistry and Physics, 16, 1603-1618,
 983 10.5194/acp-16-1603-2016, 2016.

984 Masiol, M., Squizzato, S., Formenton, G., Khan, M. B., Hopke, P. K., Nenes, A., Pandis, S. N., Tositti, L., Benetello, F., Visin, F.,
 985 and Pavoni, B.: Hybrid multiple-site mass closure and source apportionment of PM_{2.5} and aerosol acidity at major cities
 986 in the Po Valley, Science of The Total Environment, 704, 135287, <https://doi.org/10.1016/j.scitotenv.2019.135287>,
 987 2020.

988 McCormick, M. P., Thomason, L. W., and Trepte, C. R.: ATMOSPHERIC EFFECTS OF THE MT-PINATUBO ERUPTION, Nature,
 989 373, 399-404, 10.1038/373399a0, 1995.

990 [Meng, Z. Y., Seinfeld, J. H., Saxena, P., and Kim, Y. P.: Atmospheric gas-aerosol equilibrium .4. Thermodynamics of](#)
 991 [carbonates, Aerosol Science and Technology, 23, 131-154, 1995.](#)

992 [Meng, Z. Y., and Seinfeld, J. H.: Time scales to achieve atmospheric gas-aerosol equilibrium for volatile species,](#)
 993 [Atmospheric Environment, 30, 2889-2900, 10.1016/1352-2310\(95\)00493-9, 1996.](#)

994 [Metzger, S., Mihalopoulos, N., and Lelieveld, J.: Importance of mineral cations and organics in gas-aerosol partitioning of](#)
 995 [reactive nitrogen compounds: case study based on MINOS results, Atmospheric Chemistry and Physics, 6, 2549-2567,](#)
 996 [10.5194/acp-6-2549-2006, 2006.](#)

997 Nah, T., Guo, H., Sullivan, A. P., Chen, Y., Tanner, D. J., Nenes, A., Russell, A., Ng, N. L., Huey, L. G., and Weber, R. J.:
 998 Characterization of aerosol composition, aerosol acidity, and organic acid partitioning at an agriculturally intensive rural
 999 southeastern US site, Atmos. Chem. Phys., 18, 11471-11491, 10.5194/acp-18-11471-2018, 2018.

1000 Nenes, A., Pandis, S. N., Weber, R. J., and Russell, A.: Aerosol pH and liquid water content determine when particulate
 1001 matter is sensitive to ammonia and nitrate availability, Atmospheric Chemistry and Physics, 20, 3249-3258,
 1002 10.5194/acp-20-3249-2020, 2020.

1003 Oakes, M., Ingall, E. D., Lai, B., Shafer, M. M., Hays, M. D., Liu, Z. G., Russell, A. G., and Weber, R. J.: Iron Solubility Related
 1004 to Particle Sulfur Content in Source Emission and Ambient Fine Particles, Environmental Science & Technology, 46,
 1005 6637-6644, 10.1021/es300701c, 2012.

1006 Park, M., Joo, H. S., Lee, K., Jang, M., Kim, S. D., Kim, I., Borlaza, L. J. S., Lim, H., Shin, H., Chung, K. H., Choi, Y.-H., Park, S. G.,
 1007 Bae, M.-S., Lee, J., Song, H., and Park, K.: Differential toxicities of fine particulate matters from various sources,
 1008 Scientific Reports, 8, 17007, 10.1038/s41598-018-35398-0, 2018.

1009 Pathak, R. K., Yao, X. H., and Chan, C. K.: Sampling artifacts of acidity and ionic species in PM_{2.5}, Environmental Science &
 1010 Technology, 38, 254-259, 10.1021/es0342244, 2004.

1011 Pathak, R. K., Wu, W. S., and Wang, T.: Summertime PM_{2.5} ionic species in four major cities of China: nitrate
 1012 formation in an ammonia-deficient atmosphere, Atmos. Chem. Phys., 9, 1711-1722, 10.5194/acp-9-1711-2009, 2009.

1013 Petters, M. D., and Kreidenweis, S. M.: A single parameter representation of hygroscopic growth and cloud condensation
 1014 nucleus activity, Atmospheric Chemistry and Physics, 7, 1961-1971, 2007.

Formatted: Font: +Body (Calibri), 10 pt, English (United States)

Formatted: Font: +Body (Calibri), 10 pt, English (United States)

Formatted: Indent: Left: 0 cm, Hanging: 0.5 cm

015 Pozzer, A., Joeckel, P. J., Sander, R., Williams, J., Ganzeveld, L., and Lelieveld, J.: Technical note: the MESSy-submodel
016 AIRSEA calculating the air-sea exchange of chemical species, *Atmos. Chem. Phys.*, 6, 5435-5444, 2006.

017 Pozzer, A., Jockel, P., and Van Aardenne, J.: The influence of the vertical distribution of emissions on tropospheric
018 chemistry, *Atmospheric Chemistry and Physics*, 9, 9417-9432, 2009.

019 Pozzer, A., de Meij, A., Pringle, K. J., Tost, H., Doering, U. M., van Aardenne, J., and Lelieveld, J.: Distributions and regional
020 budgets of aerosols and their precursors simulated with the EMAC chemistry-climate model, *Atmos. Chem. Phys.*, 12,
021 961-987, 2012.

022 Pozzer, A., Tsimpidi, A. P., Karydis, V. A., de Meij, A., and Lelieveld, J.: Impact of agricultural emission reductions on fine-
023 particulate matter and public health, *Atmospheric Chemistry and Physics*, 17, 12813-12826, 10.5194/acp-17-12813-
024 2017, 2017.

025 Pringle, K. J., Tost, H., Message, S., Steil, B., Giannadaki, D., Nenes, A., Fountoukis, C., Stier, P., Vignati, E., and Lelieveld, J.:
026 Description and evaluation of GMX: a new aerosol submodel for global simulations (v1), *Geoscientific Model
027 Development*, 3, 391-412, 2010.

028 Pye, H. O. T., Nenes, A., Alexander, B., Ault, A. P., Barth, M. C., Clegg, S. L., Collett, J. L., Fahey, K. M., Hennigan, C. J.,
029 Herrmann, H., Kanakidou, M., Kelly, J. T., Ku, I. T., McNeill, V. F., Riemer, N., Schaefer, T., Shi, G. L., Tilgner, A., Walker, J.
030 T., Wang, T., Weber, R., Xing, J., Zaveri, R. A., and Zuend, A.: The acidity of atmospheric particles and clouds,
031 *Atmospheric Chemistry and Physics*, 20, 4809-4888, 10.5194/acp-20-4809-2020, 2020.

032 Raizenne, M., Neas, L. M., Damokosh, A. I., Dockery, D. W., Spengler, J. D., Koutrakis, P., Ware, J. H., and Speizer, F. E.:
033 Health effects of acid aerosols on North American children: Pulmonary function, *Environmental Health Perspectives*,
034 104, 506-514, 10.2307/3432991, 1996.

035 Roeckner, E., Brokopf, R., Esch, M., Giorgetta, M., Hagemann, S., Kornbluh, L., Manzini, E., Schlese, U., and Schulzweida,
036 U.: Sensitivity of simulated climate to horizontal and vertical resolution in the ECHAM5 atmosphere model, *Journal of
037 Climate*, 19, 3771-3791, 10.1175/jcli3824.1, 2006.

038 Saiz-Lopez, A., and von Glasow, R.: Reactive halogen chemistry in the troposphere, *Chemical Society Reviews*, 41, 6448-
039 6472, 10.1039/c2cs35208g, 2012.

040 Sander, R.: Compilation of Henry's law constants (version 4.0) for water as solvent, *Atmos. Chem. Phys.*, 15, 4399-4981,
041 10.5194/acp-15-4399-2015, 2015.

042 Sander, R., Baumgaertner, A., Cabrera-Perez, D., Frank, F., Gromov, S., Grooss, J. U., Harder, H., Huijnen, V., Jockel, P.,
043 Karydis, V. A., Niemeyer, K. E., Pozzer, A., Hella, R. B., Schultz, M. G., Taraborrelli, D., and Tauer, S.: The community
044 atmospheric chemistry box model CAABA/MECCA-4.0, *Geoscientific Model Development*, 12, 1365-1385, 10.5194/gmd-
045 12-1365-2019, 2019.

046 [Schaap, M., van Loon, M., ten Brink, H. M., Dentener, F. J., and Buitjes, P. J. H.: Secondary inorganic aerosol simulations for
047 Europe with special attention to nitrate, *Atmos. Chem. Phys.*, 4, 857-874, 10.5194/acp-4-857-2004, 2004.](#)

048 Seinfeld, J. H., and Pandis, S. N.: *Atmospheric Chemistry and Physics: From Air Pollution to Climate Change*, Second ed.,
049 John Wiley & Sons, Inc., Hoboken, New Jersey, 2006.

050 Shao, J., Chen, Q., Wang, Y., Lu, X., He, P., Sun, Y., Shah, V., Martin, R. V., Philip, S., Song, S., Zhao, Y., Xie, Z., Zhang, L., and
051 Alexander, B.: Heterogeneous sulfate aerosol formation mechanisms during wintertime Chinese haze events: air quality
052 model assessment using observations of sulfate oxygen isotopes in Beijing, *Atmos. Chem. Phys.*, 19, 6107-6123,
053 10.5194/acp-19-6107-2019, 2019.

054 Shi, G., Xu, J., Peng, X., Xiao, Z., Chen, K., Tian, Y., Guan, X., Feng, Y., Yu, H., Nenes, A., and Russell, A. G.: pH of Aerosols in a
055 Polluted Atmosphere: Source Contributions to Highly Acidic Aerosol, *Environmental Science & Technology*, 51, 4289-
056 4296, 10.1021/acs.est.6b05736, 2017.

057 Song, S., Gao, M., Xu, W., Shao, J., Shi, G., Wang, S., Wang, Y., Sun, Y., and McElroy, M. B.: Fine-particle pH for Beijing
058 winter haze as inferred from different thermodynamic equilibrium models, *Atmos. Chem. Phys.*, 18, 7423-7438,
059 10.5194/acp-18-7423-2018, 2018.

Formatted: Font: +Body (Calibri), 10 pt, English (United States)

Formatted: Indent: Left: 0 cm, Hanging: 0.5 cm

060 Squizzato, S., Masiol, M., Brunelli, A., Pistollato, S., Tarabotti, E., Rampazzo, G., and Pavoni, B.: Factors determining the
061 formation of secondary inorganic aerosol: a case study in the Po Valley (Italy), *Atmos. Chem. Phys.*, 13, 1927-1939,
062 10.5194/acp-13-1927-2013, 2013.

063 Sullivan, R. C., Moore, M. J. K., Petters, M. D., Kreidenweis, S. M., Roberts, G. C., and Prather, K. A.: Effect of chemical
064 mixing state on the hygroscopicity and cloud nucleation properties of calcium mineral dust particles, *Atmospheric
065 Chemistry and Physics*, 9, 3303-3316, 2009.

066 Surratt, J. D., Chan, A. W. H., Eddingsaas, N. C., Chan, M. N., Loza, C. L., Kwan, A. J., Hersey, S. P., Flagan, R. C., Wennberg, P.
067 O., and Seinfeld, J. H.: Reactive intermediates revealed in secondary organic aerosol formation from isoprene,
068 *Proceedings of the National Academy of Sciences of the United States of America*, 107, 6640-6645,
069 10.1073/pnas.0911114107, 2010.

070 Tan, T., Hu, M., Li, M., Guo, Q., Wu, Y., Fang, X., Gu, F., Wang, Y., and Wu, Z.: New insight into PM2.5 pollution patterns in
071 Beijing based on one-year measurement of chemical compositions, *Science of The Total Environment*, 621, 734-743,
072 <https://doi.org/10.1016/j.scitotenv.2017.11.208>, 2018.

073 Tost, H., Jockel, P. J., Kerkweg, A., Sander, R., and Lelieveld, J.: Technical note: A new comprehensive SCAVenging submodel
074 for global atmospheric chemistry modelling, *Atmos. Chem. Phys.*, 6, 565-574, 2006.

075 Tsimpidi, A. P., Karydis, V. A., Pozzer, A., Pandis, S. N., and Lelieveld, J.: ORACLE (v1.0): module to simulate the organic
076 aerosol composition and evolution in the atmosphere, *Geoscientific Model Development*, 7, 3153-3172, 10.5194/gmd-
077 7-3153-2014, 2014.

078 Tsimpidi, A. P., Karydis, V. A., Pandis, S. N., and Lelieveld, J.: Global combustion sources of organic aerosols: model
079 comparison with 84 AMS factor-analysis data sets, *Atmos. Chem. Phys.*, 16, 8939-8962, 10.5194/acp-16-8939-2016,
080 2016.

081 Tsimpidi, A. P., Karydis, V. A., Pozzer, A., Pandis, S. N., and Lelieveld, J.: ORACLE 2-D (v2.0): an efficient module to compute
082 the volatility and oxygen content of organic aerosol with a global chemistry-climate model, *Geoscientific Model
083 Development*, 11, 3369-3389, 10.5194/gmd-11-3369-2018, 2018.

084 van Vuuren, D. P., Edmonds, J., Kainuma, M., Riahi, K., Thomson, A., Hibbard, K., Hurtt, G. C., Kram, T., Krey, V., Lamarque,
085 J. F., Masui, T., Meinshausen, M., Nakicenovic, N., Smith, S. J., and Rose, S. K.: The representative concentration
086 pathways: an overview, *Climatic Change*, 109, 5-31, 10.1007/s10584-011-0148-z, 2011.

087 Vieira-Filho, M., Pedrotti, J. J., and Fornaro, A.: Water-soluble ions species of size-resolved aerosols: Implications for the
088 atmospheric acidity in São Paulo megacity, Brazil, *Atmospheric Research*, 181, 281-287,
089 <https://doi.org/10.1016/j.atmosres.2016.07.006>, 2016.

090 Vignati, E., Wilson, J., and Stier, P.: M7: An efficient size-resolved aerosol microphysics module for large-scale aerosol
091 transport models, *J. Geophys. Res.-Atmos.*, 109, doi: 10.1029/2003jd004485, 2004.

092 Wang, H., Ding, J., Xu, J., Wen, J., Han, J., Wang, K., Shi, G., Feng, Y., Ivey, C. E., Wang, Y., Nenes, A., Zhao, Q., and Russell, A.
093 G.: Aerosols in an arid environment: The role of aerosol water content, particulate acidity, precursors, and relative
094 humidity on secondary inorganic aerosols, *Science of The Total Environment*, 646, 564-572,
095 <https://doi.org/10.1016/j.scitotenv.2018.07.321>, 2019a.

096 Wang, Y., Li, W., Gao, W., Liu, Z., Tian, S., Shen, R., Ji, D., Wang, S., Wang, L., Tang, G., Song, T., Cheng, M., Wang, G., Gong,
097 Z., Hao, J., and Zhang, Y.: Trends in particulate matter and its chemical compositions in China from 2013–2017, *Science
098 China Earth Sciences*, 62, 1857-1871, 10.1007/s11430-018-9373-1, 2019b.

099 Weber, R. J., Guo, H. Y., Russell, A. G., and Nenes, A.: High aerosol acidity despite declining atmospheric sulfate
100 concentrations over the past 15 years, *Nature Geoscience*, 9, 282-285, 10.1038/ngeo2665, 2016.

101 Xu, L., Guo, H. Y., Boyd, C. M., Klein, M., Bougiatioti, A., Cerully, K. M., Hite, J. R., Isaacman-VanWertz, G., Kreisberg, N. M.,
102 Knote, C., Olson, K., Koss, A., Goldstein, A. H., Hering, S. V., de Gouw, J., Baumann, K., Lee, S. H., Nenes, A., Weber, R. J.,
103 and Ng, N. L.: Effects of anthropogenic emissions on aerosol formation from isoprene and monoterpenes in the
104 southeastern United States, *Proceedings of the National Academy of Sciences of the United States of America*, 112, 37-
105 42, 10.1073/pnas.1417609112, 2015.

Formatted: Font: +Body (Calibri), 10 pt, English (United States)

Formatted: Font: +Body (Calibri), 10 pt, English (United States)

Formatted: Font: +Body (Calibri), 10 pt, English (United States)

106 Xue, J., Lau, A. K. H., and Yu, J. Z.: A study of acidity on PM2.5 in Hong Kong using online ionic chemical composition
107 measurements, Atmospheric Environment, 45, 7081-7088, <https://doi.org/10.1016/j.atmosenv.2011.09.040>, 2011.

108 Yao, X., Ling, T. Y., Fang, M., and Chan, C. K.: Size dependence of in situ pH in submicron atmospheric particles in Hong
109 Kong, Atmospheric Environment, 41, 382-393, <https://doi.org/10.1016/j.atmosenv.2006.07.037>, 2007.

110 Yienger, J. J., and Levy, H.: Empirical-model of global soil-biogenic NOx emissions, Journal of Geophysical Research-
111 Atmospheres, 100, 11447-11464, 10.1029/95jd00370, 1995.

112 Zakoura, M., Kakavas, S., Nenes, A., and Pandis, S. N.: Size-resolved aerosol pH over Europe during summer, Atmos. Chem.
113 Phys. Discuss., 2020, 1-24, 10.5194/acp-2019-1146, 2020.

114 Zheng, G., Su, H., Wang, S., Andreae, M. O., Pöschl, U., and Cheng, Y.: Multiphase buffer theory explains contrasts in
115 atmospheric aerosol acidity, Science, 369, 1374-1377, 10.1126/science.aba3719, 2020.

Formatted: Font: +Body (Calibri), 10 pt, English (United States)

Formatted: Font: +Body (Calibri), 10 pt, English (United States)

Formatted: English (United States)

117 Author contributions: V.A.K. and J.L. planned the research, V.A.K., A.P.T. and A.P. performed the model calculations,
118 V.A.K., A.P., and J.L. analyzed the results, V.A.K. and J.L. wrote the paper. All authors contributed to the manuscript.:

119 Competing interests: Authors declare no competing interests. Code/Data availability: Data and related material can be
120 obtained from V.A.K. (v.karydis@fz-juelich.de) upon request.
121

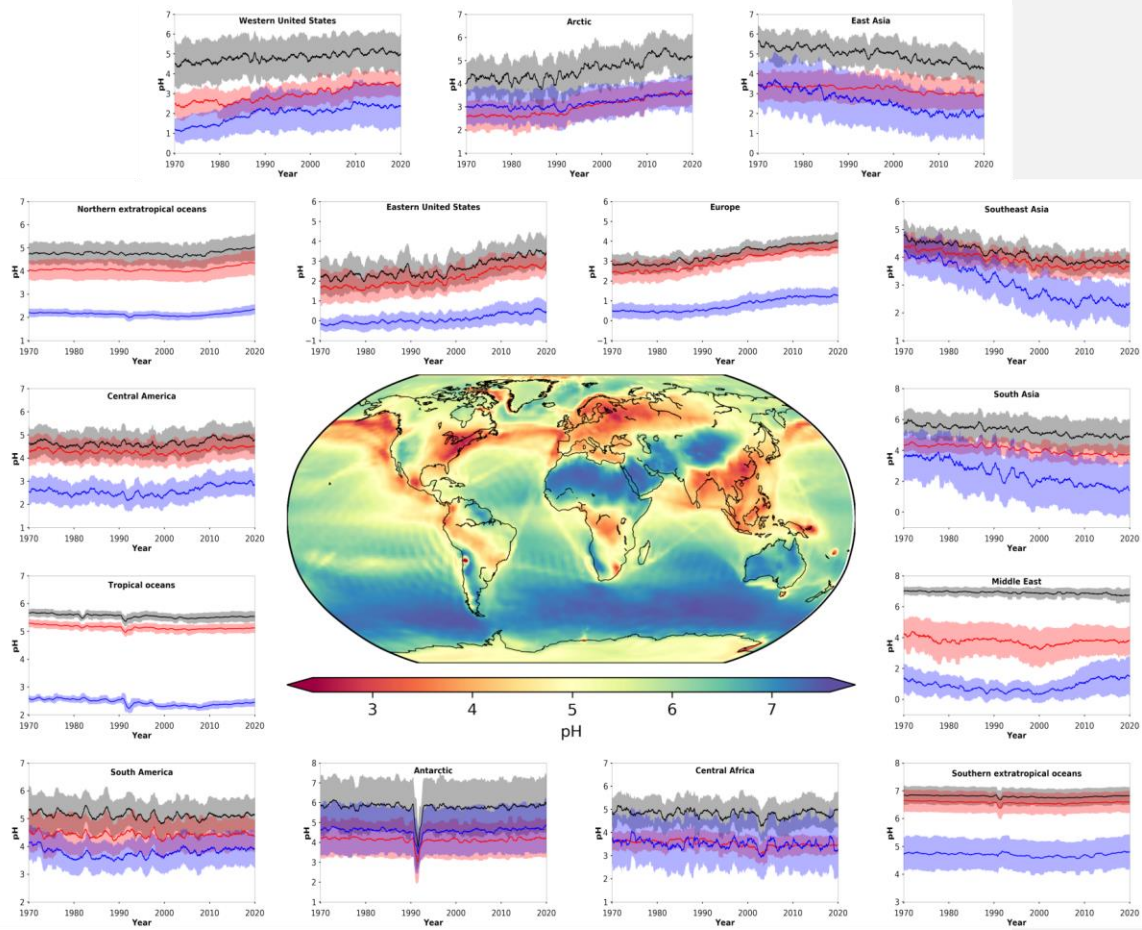
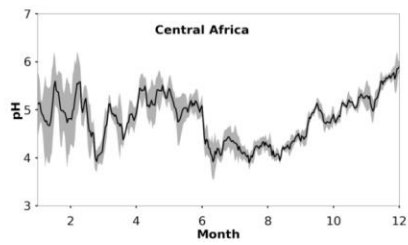
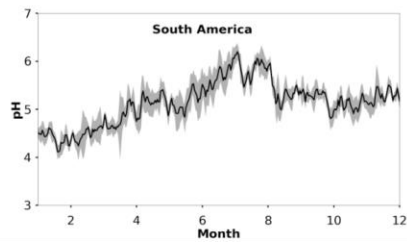
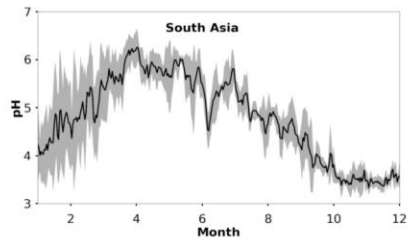
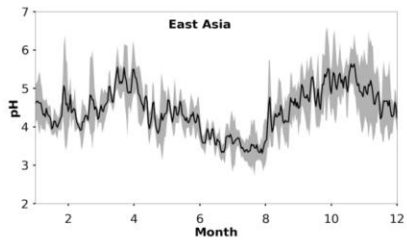
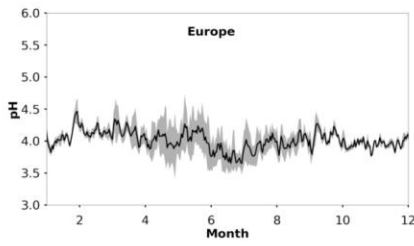
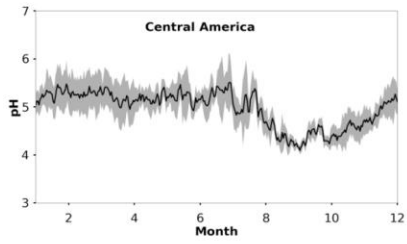
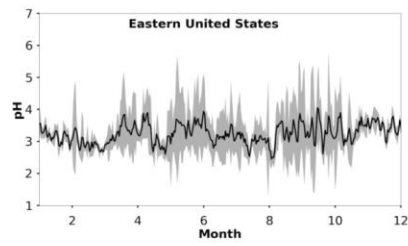
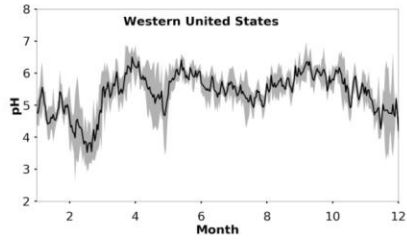


Figure 1: Mean, near-surface fine aerosol pH during the period 2010-2015 (central panel). Surrounding panels show the temporal pH evolution during the period 1970-2020 at locations defined in Table 1. Black lines represent the reference simulation. Red and blue lines show the sensitivity simulations in which crustal particle and NH₃ emissions are removed, respectively. Ranges represent the 1 σ standard deviation. The anomaly in 1991/2 is related to the Mt Pinatubo eruption.



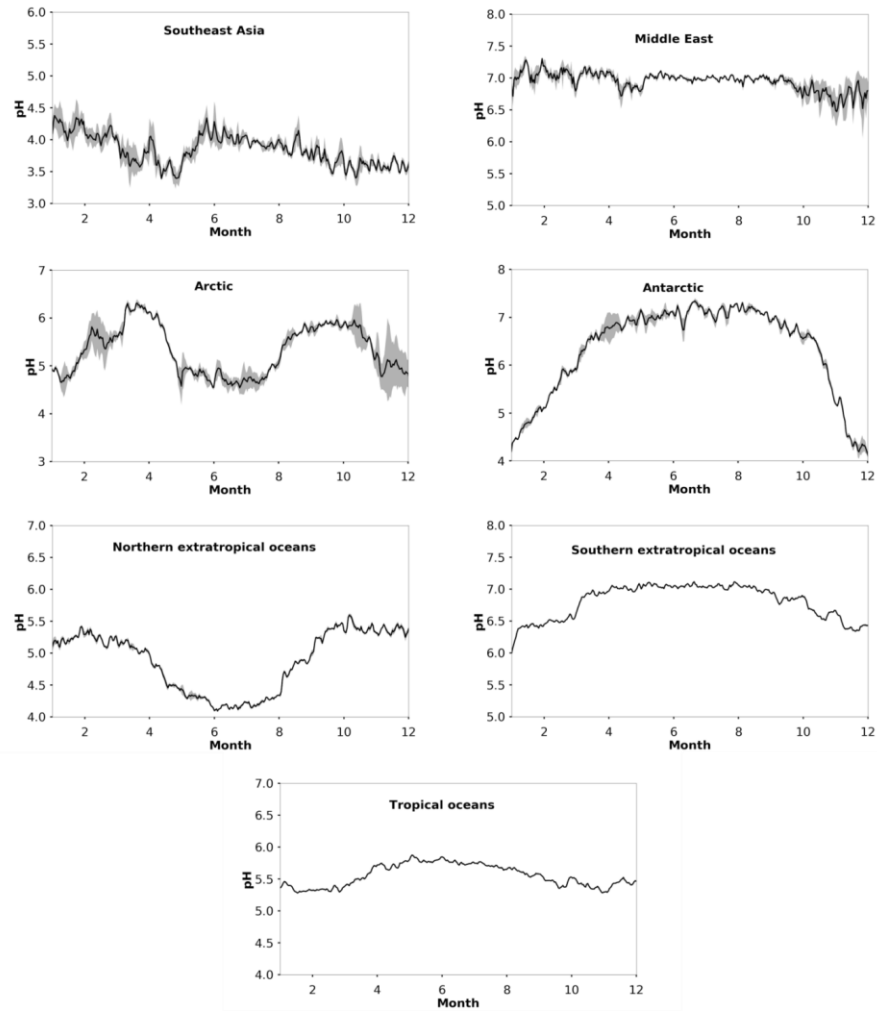


Figure 2: Average seasonal cycle of modelled pH during the period 2010-2015 at locations defined in Table 1. Ranges represent the 1 σ standard deviation.

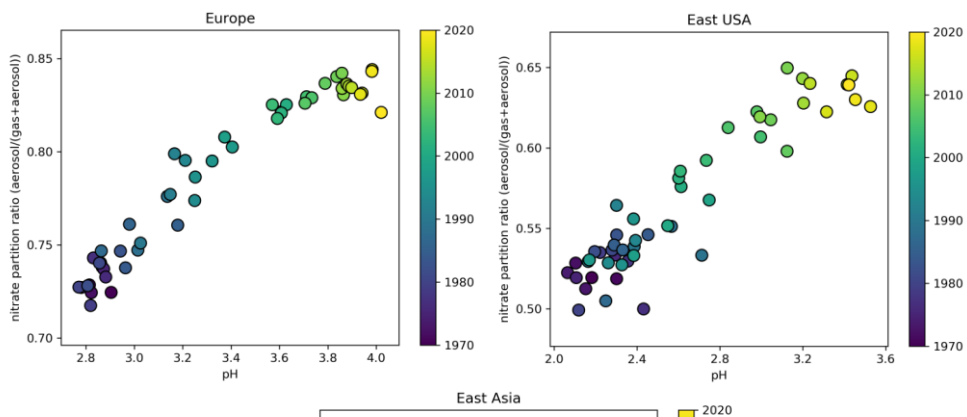


Figure 3: Time evolution of particle phase fraction of total nitrate as a function of pH over Europe (left), the Eastern USA (right) and East Asia (bottom) during the period 1970-2020.

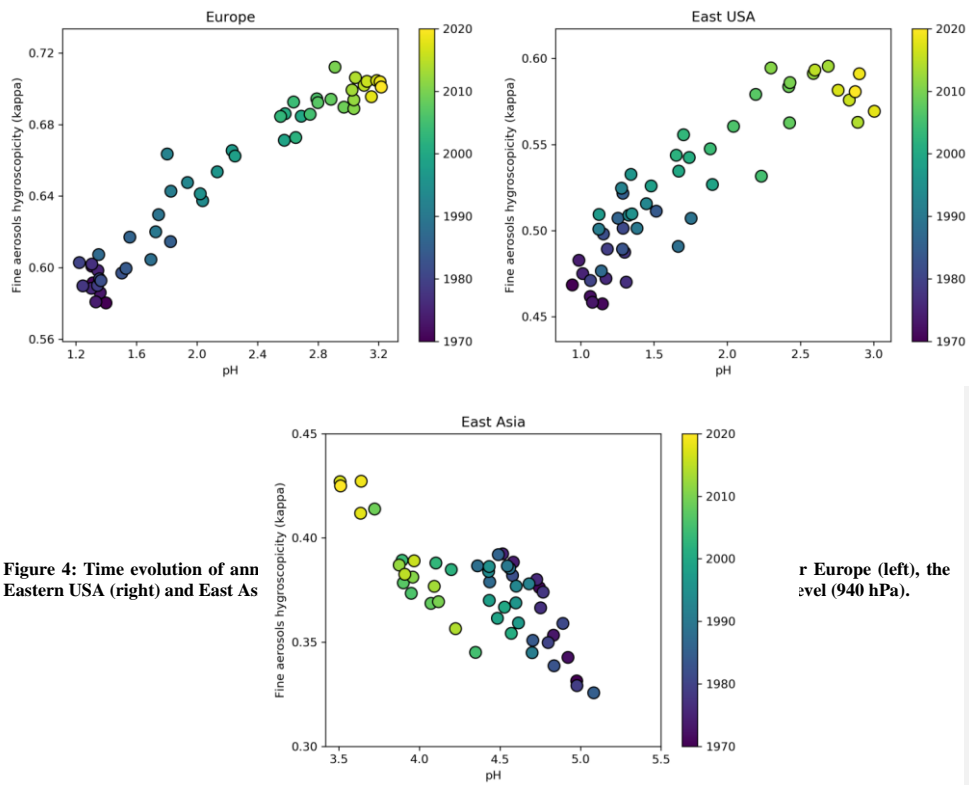


Figure 4: Time evolution of annual average fine aerosol hygroscopicity (κ) versus pH for Europe (left), the Eastern USA (right) and East Asia (bottom-left).

r Europe (left), the Eastern USA (right) and East Asia (bottom-left).

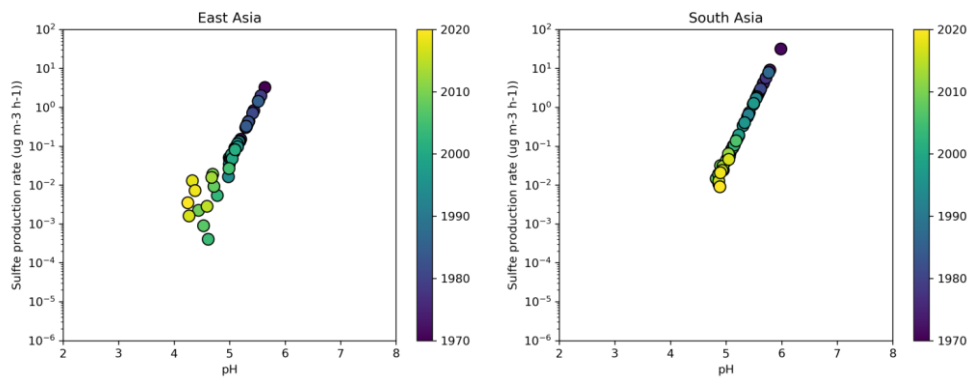


Figure 5: Time evolution of the sulfate production rate on aqueous aerosols from the SO_2+O_3 multiphase chemistry reaction as a function of aerosol pH over East Asia (left) and South Asia (right) during the period 1970-2020.

Table 1: Decadal averages of aerosol pH.

Region	Longitude	Latitude	1971-1980	1981-1990	1991-2000	2001-2010	2011-2020
Western USA ¹	90°-70°W	30°-46°N	4.6	4.8	4.8	5.0	5.1
Eastern USA ¹	124°-114°W	30°-52°N	2.2	2.4	2.4	2.9	3.3
Central America ¹	106°-52°W	4°-28°N	4.6	4.6	4.6	4.7	4.9
Europe ¹	12°W-36°E	34°-62°N	2.8	3.0	3.3	3.7	3.9
East Asia ¹	100°-114°E	20°-44°N	5.3	5.2	5.1	4.7	4.5
South Asia ¹	68°-94°E	8°-32°N	5.6	5.5	5.3	5.0	4.9
South America ¹	75°-35°W	30°-0°S	5.2	5.1	5.1	5.1	5.1
Central Africa ¹	10°-40°E	10°S-10°N	4.9	4.8	4.8	4.7	4.9
Southeast Asia ¹	94°-130°E	12°S-20°N	4.5	4.3	4.1	3.9	3.8
Middle East ¹	36°-60°E	12°-34°N	7.0	7.0	6.9	6.9	6.8
Arctic	0°-360°	60°-90°N	4.2	4.2	4.6	4.8	5.2
North extratropics ²	0°-360°	20°-60°N	4.8	4.8	4.7	4.7	4.9
Tropical oceans ²	0°-360°	20°S-20°N	5.6	5.6	5.5	5.5	5.5
South extratropics ²	0°-360°	60°-20°S	6.8	6.8	6.8	6.8	6.8
Antarctic	0°-360°	90°-60°S	5.9	5.9	5.6	5.8	5.8

¹Only values over land are considered for the calculation of pH

²Only values over oceans are considered for the calculation of pH

Supplementary Materials

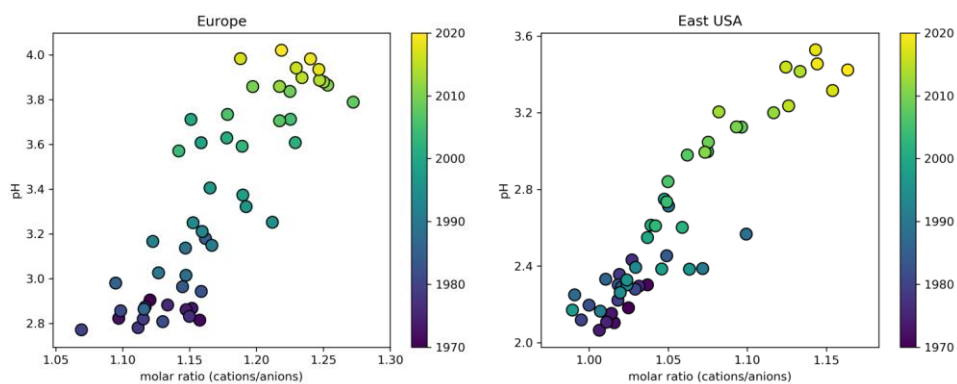


Figure S1: Time evolution of annual average pH as a function of cation/anion molar ratio over Europe (left) and the Eastern USA (right) during the period 1970-2020.

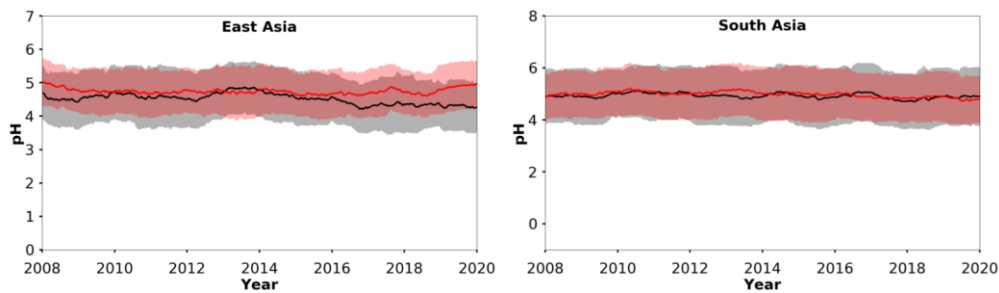


Figure S2: Temporal pH evolution in East and South Asia during the period 2008-2020. Black lines represent the reference simulation. Red lines show the sensitivity simulation in which SO₂ emissions are reduced by 75% in East Asia and increased by 50% in South Asia. Ranges represent the 1σ standard deviation.

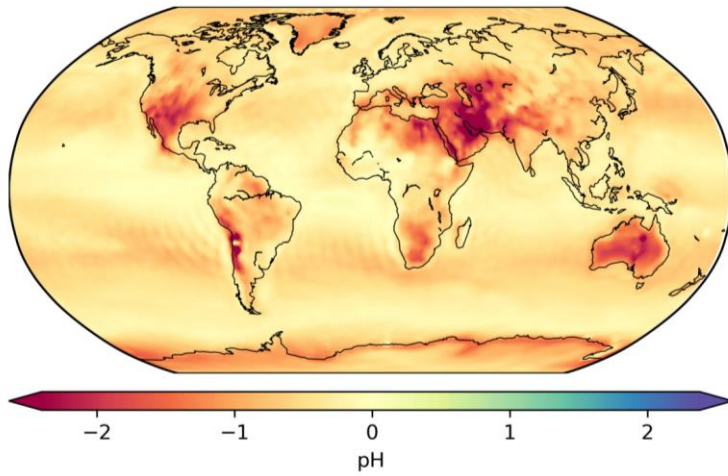


Figure S3: Absolute change in the calculated mean near-surface fine aerosol pH during the period 2010-2015 (cf. central panel in Fig. 1) by assuming that aerosols are always aqueous solution droplets (metastable state). A negative change corresponds to more acidic particles compared to the stable state assumption.

Table S1: Fractional emission factors of aerosol components for biofuel combustion, and savannah and tropical forest biomass burning (Akagi et al., 2011), and for sea salt (Seinfeld and Pandis, 2006).

Location	Latitude	Longitude	Time-period	Simulated mean-pH	Field-derived mean-pH	Method-used	Reference
Pellston, MI, USA	45.55°N	84.78°W	Jul-2016	3.8	3.5	pH-indicator paper/ colorimetric image	Craig et al., 2018
Ann Arbor, MI, USA	42.28°N	83.74°W	Aug-2016	4.3	3.5	pH-indicator paper/ colorimetric image	Craig et al., 2018
Centreville, AL, USA	32.9°N	87.25°W	Jun-1998—Aug-2013	6.4	1.2	ISORROPIA (no-NH ₃)	Weber et al., 2016
Centreville, AL, USA	32.9°N	87.25°W	Jun—Jul-2013	7.0	1.1	ISORROPIA	Pye et al., 2018
Egbert, ON, Canada	44.23°N	79.78°W	Jul—Sep-2012	3.9	2.1	E-AIM Model II	Murphy et al., 2017
Harrow, ON, Canada	42.03°N	82.89°W	Jun—Jul-2007	4.2	1.6	E-AIM Model II	Murphy et al., 2017
Pasadena, CA, USA	34.14°N	118.12°W	Jun-2010	5.9	2.7	ISORROPIA (metastable)	Guo et al., 2017
Toronto, Canada	43.66°N	79.40°W	2007-2013	4.0	2.6	E-AIM I (with gas-NH ₃ , HNO ₃)	Tao and Murphy, 2019
Toronto, Canada	43.66°N	79.40°W	2014-2016	4.1	2.7	E-AIM I (with gas-NH ₃ , HNO ₃)	Tao and Murphy, 2019
Ottawa, Canada	45.43°N	75.68°W	2007-2016	4.0	2.5	E-AIM I (with gas-NH ₃ , HNO ₃)	Tao and Murphy, 2019
Simcoe, Canada	42.86°N	80.27°W	2007-2016	4.4	2.41	E-AIM I (with gas-NH ₃ , HNO ₃)	Tao and Murphy, 2019
Montreal, Canada	45.65°N	73.57°W	2007-2016	4.0	2.4	E-AIM I (with gas-NH ₃ , HNO ₃)	Tao and Murphy, 2019
Windsor, Canada	42.29°N	83.07°W	2007-2010	4.4	2.1	E-AIM I (with gas-NH ₃ , HNO ₃)	Tao and Murphy, 2019
Windsor, Canada	42.29°N	83.07°W	2012-2016	4.5	2.4	E-AIM I (with gas-NH ₃ , HNO ₃)	Tao and Murphy, 2019
St. Anicet, Canada	45.12°N	74.29°W	2007-2016	4.0	2.5	E-AIM I (with gas-NH ₃ , HNO ₃)	Tao and Murphy, 2019
Sao Paulo, Brazil	23.55°S	46.63°W	Aug—Sep-2012	6.2	4.8	E-AIM	Vieira-Filho et al., 2016
Pe Valley, Italy	45.40°N	12.20°E	Mar-2009—Jan-2010	4.5	3.1	E-AIM Model IV	Squizzato et al., 2013

Pe-Valley, Italy	45.40°N	12.20°E	Spring-2009	4.3	3.6	E-AIM Model IV	Squizzato et al., 2013
Pe-Valley, Italy	45.40°N	12.20°E	Summer-2009	4.8	2.3	E-AIM Model IV	Squizzato et al., 2013
Pe-Valley, Italy	45.40°N	12.20°E	Fall-2009	4.5	3	E-AIM Model IV	Squizzato et al., 2013
Pe-Valley, Italy	45.40°N	12.20°E	Winter-2009-2010	4.4	3.4	E-AIM Model IV	Squizzato et al., 2013
Pe-Valley, Italy	45.40°N	12.20°E	Winter-2012-2013	4.2	3.9	ISORROPIA (metastable, no-NH ₃)	Masiol et al., 2020
Pe-Valley, Italy	45.40°N	12.20°E	Spring-2012	4.1	2.3	ISORROPIA (metastable, no-NH ₃)	Masiol et al., 2020
Cabauw, Netherlands	51.97°N	4.93°E	Jul-2012—Jun-2013	4.0	3.7	ISORROPIA	Guo et al., 2018
Cabauw, Netherlands	51.97°N	4.93°E	Jun—Aug-2013	3.6	3.3	ISORROPIA	Guo et al., 2018
Cabauw, Netherlands	51.97°N	4.93°E	Dec—Feb-2012	4.1	3.9	ISORROPIA	Guo et al., 2018
Beijing, China	39.99°N	116.30°E	Nov-2015—Dec-2016	4.9	4.2	ISORROPIA	Liu et al., 2017
Guangzhou, China	23.13°N	113.26°E	Jul-2013	2.6	2.5	E-AIM Model IV	Jia et al., 2018
Beijing, China	39.97°N	116.37°E	Nov-2014—Dec-2014	4.5	4.6	ISORROPIA	Song et al., 2018
Beijing, China	40.41°N	116.68°E	Oct-2014—Jan-2015	5.6	4.7	ISORROPIA (metastable)	He et al., 2018
Beijing, China	39.99°N	116.31°E	Jan—Dec-2014	4.9	3.0	ISORROPIA (metastable)	Tan et al., 2018
Beijing, China	39.99°N	116.31°E	Winter-2014	5.5	4.1	ISORROPIA (metastable)	Tan et al., 2018
Beijing, China	39.99°N	116.31°E	Fall-2014	6.0	3.1	ISORROPIA (metastable)	Tan et al., 2018
Beijing, China	39.99°N	116.31°E	Spring-2014	5.4	2.1	ISORROPIA (metastable)	Tan et al., 2018
Beijing, China	39.99°N	116.31°E	Summer-2014	3.1	1.8	ISORROPIA (metastable)	Tan et al., 2018
Tianjin, China	39.11°N	117.16°E	Dec-2014—Jun-2015	4.4	4.9	ISORROPIA (metastable)	Shi et al., 2017

Tianjin, China	39.11°N	117.16°E	Aug-2015	1-4	3-4	ISORROPIA (metastable)	Shi et al., 2017
Beijing, China	39.98°N	116.28°E	Feb-2017	4-7	4-5	ISORROPIA	Ding et al., 2019
Beijing, China	39.98°N	116.28°E	Apr—May-2016	5-2	4-4	ISORROPIA	Ding et al., 2019
Beijing, China	39.98°N	116.28°E	Jul—Aug-2017	2-2	3-8	ISORROPIA	Ding et al., 2019
Beijing, China	39.98°N	116.28°E	Sep—Oct-2017	4-5	4-3	ISORROPIA	Ding et al., 2019
Guangzhou, China	23.13°N	113.26°E	Jul—Sep-2013	2-7	2-4	E-AIM Model III	Jia et al., 2018
Hohhot, China	40.48°N	111.41°E	Summer-2014	5-5	5	ISORROPIA (metastable, no-NH ₃)	Wang et al., 2019
Hohhot, China	40.48°N	111.41°E	Autumn-2014	6-8	5-3	ISORROPIA (metastable, no-NH ₃)	Wang et al., 2019
Hohhot, China	40.48°N	111.41°E	Winter-2014	5-8	5-7	ISORROPIA (metastable, no-NH ₃)	Wang et al., 2019
Hohhot, China	40.48°N	111.41°E	Spring-2015	6-1	6-1	ISORROPIA (metastable, no-NH ₃)	Wang et al., 2019
Hohhot, China	40.48°N	111.41°E	2014—2015	6-2	5-6	ISORROPIA (metastable, no-NH ₃)	Wang et al., 2019
Beijing, China	40.41°N	116.68°E	Oct-2014—Jan-2015	5-6	7-6	ISORROPIA (stable state)	He et al., 2018
Xi'an, China	34.23°N	108.89°E	Nov—Dec-2012	5-7	6-7	ISORROPIA	Wang et al., 2016
Beijing, China	39.99°N	116.30°E	Jan—Feb-2015	5-0	7-6	ISORROPIA	Wang et al., 2016
Beijing, China	40.35°N	116.30°E	Jun—Aug-2005	4-2	0-6	E-AIM Model II (only aerosols)	Pathak et al., 2009
Shanghai, China	31.45°N	121.10°E	May—Jun-2005	3-5	0-7	E-AIM Model II (only aerosols)	Pathak et al., 2009
Lanzhou, China	36.13°N	103.68°E	Jun—Jul-2006	6-8	0-6	E-AIM Model II (only aerosols)	Pathak et al., 2009
Beijing, China	40.32°N	116.32°E	Jan-2005—Apr-2006	5-1	0-7	E-AIM Model II (only aerosols)	He et al., 2012
Chongqing, China	29.57°N	106.53°E	Jan-2005—Apr-2006	3-6	1-5	E-AIM Model II (only aerosols)	He et al., 2012

Beijing, China	40°N	116.33°E	Jan-2013	4.6	5.8	ISORROPIA (forward & reverse, estimated-NH ₃)	Wang et al., 2016
Singapore	1.3°N	103.78°E	Sep—Nov-2011	3.2	0.6	E-AIM Model IV	Behara et al., 2013
Hong-Kong	22.34°N	114.26°E	Jul-1997—May-1998	3.3	0.3	E-AIM Model II (for RH >= 70%)	Yao et al., 2007
Hong-Kong	22.34°N	114.26°E	Nov-1996—Nov-1997	3.4	-1	E-AIM Model II (for RH < 70%)	Yao et al., 2007
Hong-Kong	22.34°N	114.26°E	Oct-2008	5.0	0.6	E-AIM Model III (only-aerosols)	Xue et al., 2011
Hong-Kong	22.34°N	114.26°E	Nov-2008	3.7	-0.5	E-AIM Model III (only-aerosols)	Xue et al., 2011
Hong-Kong	22.34°N	114.26°E	Jun—Jul-2009	1.6	-0.1	E-AIM Model III (only-aerosols)	Xue et al., 2011
Pacific Ocean	47.5°S	147.5°E	Nov—Dec-1995	7.0	1.0	EQUISOLV	Fridlind and Jacobson, 2000
South Ocean	61°S	45°W	Jan-2015	6.9	1.4	ISORROPIA (no-NH ₃)	Dall'Osto et al., 2019
South Ocean	64°S	65°W	Jan—Feb-2015	6.9	3.8	ISORROPIA (no-NH ₃)	Dall'Osto et al., 2019

Table S2: Fractional emission factors of aerosol components for biofuel combustion, and savannah and tropical forest biomass burning (Alkagi et al., 2011), and for sea salt (Seinfeld and Pandis, 2006).

Source	SO ₄ ²⁻	NO ₃ ⁻	Cl ⁻	Na ⁺	K ⁺	Mg ²⁺	Ca ²⁺	NH ₄ ⁺
Biofuel combustion	-	0.01	-	-	0.09	0.02	0.07	-
Grassfire burning	0.05	0.04	0.62	0.01	0.62	0.04	0.06	0.01
Forest fire burning	0.25	0.21	0.29	0.01	0.56	0.08	0.16	0.01
Sea salt	0.07	-	0.55	0.30	0.01	0.03	0.01	-
	7			6	1	7	2	

Table S3: Fractional chemical composition of mineral dust emissions (Karydis et al., 2016).

Desert	Na ⁺	K ⁺	Ca ²⁺	Mg ²⁺	Other
Great Basin	0.064	0.023	0.053	0.018	0.842
Mojave	0.015	0.027	0.059	0.019	0.880
Sonoran	0.025	0.012	0.037	0.006	0.920
Patagonia	0.012	0.015	0.021	0.013	0.939
Monte	0.023	0.018	0.025	0.009	0.925
Atacama	0.069	0.007	0.018	0.005	0.901
Kalahari/ Namibia	0.030	0.050	0.120	0.090	0.710
Sahara	0.011	0.035	0.075	0.030	0.849
Saudi Arabia	0.010	0.004	0.034	0.006	0.946
Thar/Lut	0.022	0.033	0.082	0.022	0.841
Taklimakan	0.012	0.030	0.120	0.028	0.810
Gobi	0.012	0.021	0.077	0.017	0.873
Great Sandy/ Simpson	0.028	0.001	0.005	0.003	0.963
Other	0.012	0.015	0.024	0.009	0.940

Formatted: Font: 9 pt

Formatted: Indent: Left: 0 cm, Hanging: 0.63 cm, Tab stops: Not at 3.23 cm

Supplementary Materials

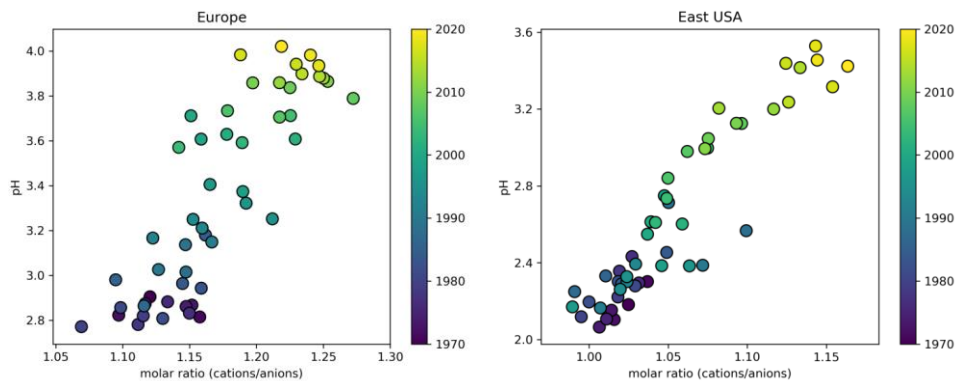


Figure S1: Time evolution of annual average pH as a function of cation/anion molar ratio over Europe (left) and the Eastern USA (right) during the period 1970-2020. The calculated ratio includes all ions from both solid salts and the liquid phase.

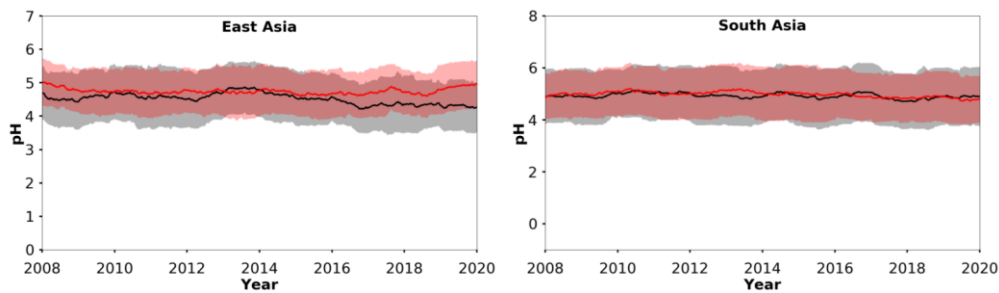


Figure S2: Temporal pH evolution in East and South Asia during the period 2008-2020. Black lines represent the reference simulation. Red lines show the sensitivity simulation in which SO₂ emissions are reduced by 75% in East Asia and increased by 50% in South Asia. Ranges represent the 1 σ standard deviation.

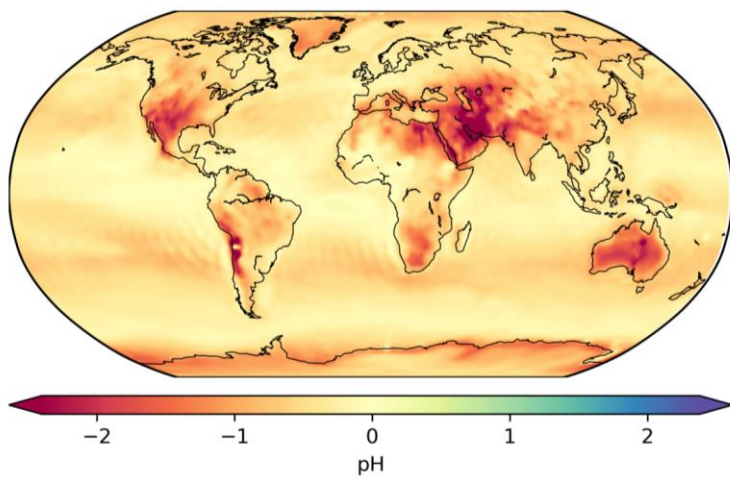


Figure S3: Absolute change in the calculated mean near-surface fine aerosol pH during the period 2010-2015 (cf. central panel in Fig. 1) by assuming that aerosols are always aqueous solution droplets (metastable state). A negative change corresponds to more acidic particles compared to the stable state assumption.

Table S1: Simulated fine aerosol pH compared to observationally-constrained estimates of fine aerosol acidity compiled by Pye et al. (2020).

Location	Latitude	Longitude	Time period	Simulated mean pH (Stable)	Simulated mean pH (Metastable)	Field derived mean pH	Method used	Reference
Pellston, MI, USA	45.55°N	84.78°W	Jul 2016	3.8	3.1	3.5	pH indicator paper/ colorimetric image	Craig et al. (2018)
Ann Arbor, MI, USA	42.28°N	83.74°W	Aug 2016	4.3	3.0	3.5	pH indicator paper/ colorimetric image	Craig et al. (2018)
Centreville, AL, USA	32.9°N	87.25°W	Jun 1998 – Aug 2013	6.4	5.7	1.2	ISORROPIA (no NH ₃)	Weber et al. (2016)
Centreville, AL, USA	32.9°N	87.25°W	Jun – Jul 2013	7.0	6.5	1.1	ISORROPIA	Pye et al. (2018)
Egbert, ON, Canada	44.23°N	79.78°W	Jul – Sep 2012	3.9	3.5	2.1	E-AIM Model II	Murphy et al. (2017)
Harrow, ON, Canada	42.03°N	82.89°W	Jun – Jul 2007	4.2	3.0	1.6	E-AIM Model II	Murphy et al. (2017)
Pasadena, CA, USA	34.14°N	118.12°W	Jun 2010	5.9	2.7	2.7	ISORROPIA (metastable)	Guo et al. (2017)
Toronto, Canada	43.66°N	79.40°W	2007-2013	4.0	3.6	2.6	E-AIM I (with gas NH ₃ , HNO ₃)	Tao and Murphy (2019)
Toronto, Canada	43.66°N	79.40°W	2014-2016	4.1	3.7	2.7	E-AIM I (with gas NH ₃ , HNO ₃)	Tao and Murphy (2019)
Ottawa, Canada	45.43°N	75.68°W	2007-2016	4.0	3.9	2.5	E-AIM I (with gas NH ₃ , HNO ₃)	Tao and Murphy (2019)
Simcoe, Canada	42.86°N	80.27°W	2007-2016	4.4	3.7	2.41	E-AIM I (with gas NH ₃ , HNO ₃)	Tao and Murphy (2019)
Montreal, Canada	45.65°N	73.57°W	2007-2016	4.0	3.9	2.4	E-AIM I (with gas NH ₃ , HNO ₃)	Tao and Murphy (2019)
Windsor, Canada	42.29°N	83.07°W	2007-2010	4.4	3.6	2.1	E-AIM I (with gas NH ₃ , HNO ₃)	Tao and Murphy (2019)
Windsor, Canada	42.29°N	83.07°W	2012-2016	4.5	3.7	2.4	E-AIM I (with gas NH ₃ , HNO ₃)	Tao and Murphy (2019)
St. Anicet, Canada	45.12°N	74.29°W	2007-2016	4.0	3.9	2.5	E-AIM I (with gas NH ₃ , HNO ₃)	Tao and Murphy (2019)
Sao Paulo, Brazil	23.55°S	46.63°W	Aug – Sep 2012	6.2	6.1	4.8	E-AIM	Vieira-Filho et al. (2016)
Po Valley, Italy	45.40°N	12.20°E	Mar 2009 – Jan 2010	4.5	3.6	3.1	E-AIM Model IV	Squizzato et al. (2013)
Po Valley, Italy	45.40°N	12.20°E	Spring 2009	4.3	3.7	3.6	E-AIM Model IV	Squizzato et al. (2013)
Po Valley, Italy	45.40°N	12.20°E	Summer 2009	4.8	3.0	2.3	E-AIM Model IV	Squizzato et al. (2013)
Po Valley, Italy	45.40°N	12.20°E	Fall 2009	4.5	3.6	3	E-AIM Model IV	Squizzato et al.

Italy								(2013)
Po Valley, Italy	45.40°N	12.20°E	Winter 2009-2010	4.4	4.0	3.4	E-AIM Model IV	Squizzato et al. (2013)
Po Valley, Italy	45.40°N	12.20°E	Winter 2012-2013	4.2	4.0	3.9	ISORROPIA (metastable, no NH ₃)	Masiol et al. (2020)
Po Valley, Italy	45.40°N	12.20°E	Spring 2012	4.1	3.1	2.3	ISORROPIA (metastable, no NH ₃)	Masiol et al. (2020)
Cabauw, Netherlands	51.97°N	4.93°E	Jul 2012 – Jun 2013	4.0	3.8	3.7	ISORROPIA	Guo et al. (2018)
Cabauw, Netherlands	51.97°N	4.93°E	Jun – Aug 2013	3.6	3.4	3.3	ISORROPIA	Guo et al. (2018)
Cabauw, Netherlands	51.97°N	4.93°E	Dec – Feb 2012	4.1	4.1	3.9	ISORROPIA	Guo et al. (2018)
Beijing, China	39.99°N	116.30°E	Nov 2015 – Dec 2016	4.9	4.2	4.2	ISORROPIA	Liu et al. (2017)
Guangzhou, China	23.13°N	113.26°E	Jul 2013	2.6	1.9	2.5	E-AIM Model IV	Jia et al. (2018)
Beijing, China	39.97°N	116.37°E	Nov 2014 – Dec 2014	4.5	5.3	4.6	ISORROPIA	Song et al. (2018)
Beijing, China	40.41°N	116.68°E	Oct 2014 – Jan 2015	5.6	4.9	4.7	ISORROPIA (metastable)	He et al. (2018)
Beijing, China	39.99°N	116.31°E	Jan – Dec 2014	4.9	4.0	3.0	ISORROPIA (metastable)	Tan et al. (2018)
Beijing, China	39.99°N	116.31°E	Winter 2014	5.5	4.4	4.1	ISORROPIA (metastable)	Tan et al. (2018)
Beijing, China	39.99°N	116.31°E	Fall 2014	6.0	4.6	3.1	ISORROPIA (metastable)	Tan et al. (2018)
Beijing, China	39.99°N	116.31°E	Spring 2014	5.4	4.5	2.1	ISORROPIA (metastable)	Tan et al. (2018)
Beijing, China	39.99°N	116.31°E	Summer 2014	3.1	2.4	1.8	ISORROPIA (metastable)	Tan et al. (2018)
Tianjin, China	39.11°N	117.16°E	Dec 2014 – Jun 2015	4.4	3.7	4.9	ISORROPIA (metastable)	Shi et al. (2017)
Tianjin, China	39.11°N	117.16°E	Aug 2015	1.4	1.2	3.4	ISORROPIA (metastable)	Shi et al. (2017)
Beijing, China	39.98°N	116.28°E	Feb 2017	4.7	4.8	4.5	ISORROPIA	Ding et al. (2019)
Beijing, China	39.98°N	116.28°E	Apr - May 2016	5.2	4.7	4.4	ISORROPIA	Ding et al. (2019)
Beijing, China	39.98°N	116.28°E	Jul - Aug 2017	2.2	1.9	3.8	ISORROPIA	Ding et al. (2019)
Beijing, China	39.98°N	116.28°E	Sep - Oct 2017	4.5	3.7	4.3	ISORROPIA	Ding et al. (2019)

Guangzhou, China	23.13°N	113.26°E	Jul – Sep 2013	2.7	2.2	2.4	E-AIM Model III	Jia et al. (2018)
Hohhot, China	40.48°N	111.41°E	Summer 2014	5.5	4.0	5	ISORROPIA (metastable, no NH ₃)	Wang et al., 2019
Hohhot, China	40.48°N	111.41°E	Autumn 2014	6.8	5.3	5.3	ISORROPIA (metastable, no NH ₃)	Wang et al. (2019)
Hohhot, China	40.48°N	111.41°E	Winter 2014	5.8	5.0	5.7	ISORROPIA (metastable, no NH ₃)	Wang et al. (2019)
Hohhot, China	40.48°N	111.41°E	Spring 2015	6.1	5.1	6.1	ISORROPIA (metastable, no NH ₃)	Wang et al. (2019)
Hohhot, China	40.48°N	111.41°E	2014 - 2015	6.2	5.0	5.6	ISORROPIA (metastable, no NH ₃)	Wang et al. (2019)
Beijing, China	40.41°N	116.68°E	Oct 2014 – Jan 2015	5.6	4.9	7.6	ISORROPIA (stable state)	He et al. (2018)
Xi'an, China	34.23°N	108.89°E	Nov – Dec 2012	5.7	4.5	6.7	ISORROPIA	Wang et al. (2016)
Beijing, China	39.99°N	116.30°E	Jan – Feb 2015	5.0	3.8	7.6	ISORROPIA	Wang et al. (2016)
Beijing, China	40.35°N	116.30°E	Jun – Aug 2005	4.2	3.3	0.6	E-AIM Model II (only aerosols)	Pathak et al. (2009)
Shanghai, China	31.45°N	121.10°E	May – Jun 2005	3.5	3.1	0.7	E-AIM Model II (only aerosols)	Pathak et al. (2009)
Lanzhou, China	36.13°N	103.68°E	Jun – Jul 2006	6.8	5.1	0.6	E-AIM Model II (only aerosols)	Pathak et al. (2009)
Beijing, China	40.32°N	116.32°E	Jan 2005 – Apr 2006	5.1	<u>4.1</u>	0.7	E-AIM Model II (only aerosols)	He et al. (2012)
Chongqing, China	29.57°N	106.53°E	Jan 2005 – Apr 2006	3.6	<u>2.7</u>	1.5	E-AIM Model II (only aerosols)	He et al. (2012)
Beijing, China	40°N	116.33°E	Jan 2013	4.6	<u>4.5</u>	5.8	ISORROPIA (forward & reverse, estimated NH ₃)	Wang et al. (2016)
Singapore	1.3°N	103.78°E	Sep – Nov 2011	3.2	3.0	0.6	E-AIM Model IV	Behera et al. (2013)
Hong Kong	22.34°N	114.26°E	Jul 1997 – May 1998	3.3	3.0	0.3	E-AIM Model II (for RH ≥ 70%)	Yao et al. (2007)
Hong Kong	22.34°N	114.26°E	Nov 1996 – Nov 1997	3.4	2.9	-1	E-AIM Model II (for RH < 70%)	Yao et al. (2007)
Hong Kong	22.34°N	114.26°E	Oct 2008	5.0	<u>3.2</u>	0.6	E-AIM Model III (only aerosols)	Xue et al. (2011)
Hong Kong	22.34°N	114.26°E	Nov 2008	3.7	<u>2.7</u>	-0.5	E-AIM Model III (only aerosols)	Xue et al. (2011)
Hong Kong	22.34°N	114.26°E	Jun - Jul 2009	1.6	<u>2.0</u>	-0.1	E-AIM Model III (only aerosols)	Xue et al. (2011)
Pacific Ocean	47.5°S	147.5°E	Nov - Dec 1995	7.0	6.5	1.0	EQUISOLV	Fridlind and Jacobson (2000)

South Ocean	61°S	45°W	Jan 2015	6.9	6.7	1.4	ISORROPIA (no NH ₃)	Dall'Osto et al. (2019)
South Ocean	64°S	65°W	Jan – Feb 2015	6.9	6.8	3.8	ISORROPIA (no NH ₃)	Dall'Osto et al. (2019)

Table S2: Fractional emission factors of aerosol components for biofuel combustion, and savannah and tropical forest biomass burning (Akagi et al., 2011), and for sea salt (Seinfeld and Pandis, 2006).

Source	SO ₄ ²⁻	NO ₃ ⁻	Cl ⁻	Na ⁺	K ⁺	Mg ²⁺	Ca ²⁺	NH ₄ ⁺
Biofuel combustion	-	0.01	-	-	0.09	0.02	0.07	-
Grassfire burning	0.05	0.04	0.62	0.01	0.62	0.04	0.06	0.01
Forest fire burning	0.25	0.21	0.29	0.01	0.56	0.08	0.16	0.01
Sea salt	0.07	-	0.55	0.30	0.01	0.03	0.01	-
	7			6	1	7	2	

Table S3: Fractional chemical composition of mineral dust emissions (Karydis et al., 2016).

Desert	Na ⁺	K ⁺	Ca ²⁺	Mg ²⁺	Other
Great Basin	0.064	0.023	0.053	0.018	0.842
Mojave	0.015	0.027	0.059	0.019	0.880
Sonoran	0.025	0.012	0.037	0.006	0.920
Patagonia	0.012	0.015	0.021	0.013	0.939
Monte	0.023	0.018	0.025	0.009	0.925
Atacama	0.069	0.007	0.018	0.005	0.901
Kalahari/ Namibia	0.030	0.050	0.120	0.090	0.710
Sahara	0.011	0.035	0.075	0.030	0.849
Saudi Arabia	0.010	0.004	0.034	0.006	0.946
Thar/Lut	0.022	0.033	0.082	0.022	0.841
Taklimakan	0.012	0.030	0.120	0.028	0.810
Gobi	0.012	0.021	0.077	0.017	0.873
Great Sandy/ Simpson	0.028	0.001	0.005	0.003	0.963
Other	0.012	0.015	0.024	0.009	0.940

Formatted Table

References

- Akagi, S. K., Yokelson, R. J., Wiedinmyer, C., Alvarado, M. J., Reid, J. S., Karl, T., Crouse, J. D., and Wennberg, P. O.: Emission factors for open and domestic biomass burning for use in atmospheric models, *Atmos. Chem. Phys.*, 11, 4039-4072, 10.5194/acp-11-4039-2011, 2011.
- Behera, S. N., Betha, R., Liu, P., and Balasubramanian, R.: A study of diurnal variations of PM_{2.5} acidity and related chemical species using a new thermodynamic equilibrium model, *Science of The Total Environment*, 452-453, 286-295, <https://doi.org/10.1016/j.scitotenv.2013.02.062>, 2013.
- Craig, R. L., Peterson, P. K., Nandy, L., Lei, Z., Hossain, M. A., Camarena, S., Dodson, R. A., Cook, R. D., Dutcher, C. S., and Ault, A. P.: Direct Determination of Aerosol pH: Size-Resolved Measurements of Submicrometer and Supermicrometer Aqueous Particles, *Analytical Chemistry*, 90, 11232-11239, 10.1021/acs.analchem.8b00586, 2018.
- Dall'Osto, M., Airs, R. L., Beale, R., Cree, C., Fitzsimons, M. F., Beddows, D., Harrison, R. M., Ceburnis, D., O'Dowd, C., Rinaldi, M., Paglione, M., Nenes, A., Decesari, S., and Simó, R.: Simultaneous Detection of Alkylamines in the Surface Ocean and Atmosphere of the Antarctic Sympagic Environment, *ACS Earth and Space Chemistry*, 3, 854-862, 10.1021/acsearthspacechem.9b00028, 2019.
- Ding, J., Zhao, P., Su, J., Dong, Q., Du, X., and Zhang, Y.: Aerosol pH and its driving factors in Beijing, *Atmos. Chem. Phys.*, 19, 7939-7954, 10.5194/acp-19-7939-2019, 2019.
- Fridlind, A. M., and Jacobson, M. Z.: A study of gas-aerosol equilibrium and aerosol pH in the remote marine boundary layer during the First Aerosol Characterization Experiment (ACE 1), *Journal of Geophysical Research: Atmospheres*, 105, 17325-17340, <https://doi.org/10.1029/2000JD900209>, 2000.

Field Code Changed

Formatted: English (United States)

Field Code Changed

Formatted: English (United States)

- Guo, H., Otjes, R., Schlag, P., Kiendler-Scharr, A., Nenes, A., and Weber, R. J.: Effectiveness of ammonia reduction on control of fine particle nitrate, *Atmospheric Chemistry and Physics*, 18, 12241-12256, 10.5194/acp-18-12241-2018, 2018.
- Guo, H. Y., Liu, J. M., Froyd, K. D., Roberts, J. M., Veres, P. R., Hayes, P. L., Jimenez, J. L., Nenes, A., and Weber, R. J.: Fine particle pH and gas-particle phase partitioning of inorganic species in Pasadena, California, during the 2010 CalNex campaign, *Atmospheric Chemistry and Physics*, 17, 5703-5719, 10.5194/acp-17-5703-2017, 2017.
- He, K., Zhao, Q., Ma, Y., Duan, F., Yang, F., Shi, Z., and Chen, G.: Spatial and seasonal variability of PM_{2.5} acidity at two Chinese megacities: insights into the formation of secondary inorganic aerosols, *Atmos. Chem. Phys.*, 12, 1377-1395, 10.5194/acp-12-1377-2012, 2012.
- He, P., Alexander, B., Geng, L., Chi, X., Fan, S., Zhan, H., Kang, H., Zheng, G., Cheng, Y., Su, H., Liu, C., and Xie, Z.: Isotopic constraints on heterogeneous sulfate production in Beijing haze, *Atmos. Chem. Phys.*, 18, 5515-5528, 10.5194/acp-18-5515-2018, 2018.
- Jia, S., Wang, X., Zhang, Q., Sarkar, S., Wu, L., Huang, M., Zhang, J., and Yang, L.: Technical note: Comparison and interconversion of pH based on different standard states for aerosol acidity characterization, *Atmos. Chem. Phys.*, 18, 11125-11133, 10.5194/acp-18-11125-2018, 2018.
- Karydis, V. A., Tsimpidi, A. P., Pozzer, A., Astitha, M., and Lelieveld, J.: Effects of mineral dust on global atmospheric nitrate concentrations, *Atmos. Chem. Phys.*, 16, 1491-1509, 10.5194/acp-16-1491-2016, 2016.
- Liu, M., Song, Y., Zhou, T., Xu, Z., Yan, C., Zheng, M., Wu, Z., Hu, M., Wu, Y., and Zhu, T.: Fine particle pH during severe haze episodes in northern China, *Geophysical Research Letters*, 44, 5213-5221, <https://doi.org/10.1002/2017GL073210>, 2017.
- Masiol, M., Squizzato, S., Formenton, G., Khan, M. B., Hopke, P. K., Nenes, A., Pandis, S. N., Tositti, L., Benetello, F., Visin, F., and Pavoni, B.: Hybrid multiple-site mass closure and source apportionment of PM_{2.5} and aerosol acidity at major cities in the Po Valley, *Science of The Total Environment*, 704, 135287, <https://doi.org/10.1016/j.scitotenv.2019.135287>, 2020.
- Murphy, J. G., Gregoire, P. K., Tevlin, A. G., Wentworth, G. R., Ellis, R. A., Markovic, M. Z., and VandenBoer, T. C.: Observational constraints on particle acidity using measurements and modelling of particles and gases, *Faraday Discussions*, 200, 379-395, 10.1039/C7FD00086C, 2017.
- Pathak, R. K., Wu, W. S., and Wang, T.: Summertime PM_{2.5} ionic species in four major cities of China: nitrate formation in an ammonia-deficient atmosphere, *Atmos. Chem. Phys.*, 9, 1711-1722, 10.5194/acp-9-1711-2009, 2009.
- Pye, H. O. T., Zuend, A., Fry, J. L., Isaacman-VanWertz, G., Capps, S. L., Appel, K. W., Foroutan, H., Xu, L., Ng, N. L., and Goldstein, A. H.: Coupling of organic and inorganic aerosol systems and the effect on gas-particle partitioning in the southeastern US, *Atmos. Chem. Phys.*, 18, 357-370, 10.5194/acp-18-357-2018, 2018.
- Pye, H. O. T., Nenes, A., Alexander, B., Ault, A. P., Barth, M. C., Clegg, S. L., Collett, J. L., Fahey, K. M., Hennigan, C. J., Herrmann, H., Kanakidou, M., Kelly, J. T., Ku, I. T., McNeill, V. F., Riemer, N., Schaefer, T., Shi, G. L., Tilgner, A., Walker, J. T., Wang, T., Weber, R., Xing, J., Zaveri, R. A., and Zuend, A.: The acidity of atmospheric particles and clouds, *Atmospheric Chemistry and Physics*, 20, 4809-4888, 10.5194/acp-20-4809-2020, 2020.
- Seinfeld, J. H., and Pandis, S. N.: *Atmospheric Chemistry and Physics: From Air Pollution to Climate Change*, Second ed., John Wiley & Sons, Inc., Hoboken, New Jersey, 2006.
- Shi, G., Xu, J., Peng, X., Xiao, Z., Chen, K., Tian, Y., Guan, X., Feng, Y., Yu, H., Nenes, A., and Russell, A. G.: pH of Aerosols in a Polluted Atmosphere: Source Contributions to Highly Acidic Aerosol, *Environmental Science & Technology*, 51, 4289-4296, 10.1021/acs.est.6b05736, 2017.
- Song, S., Gao, M., Xu, W., Shao, J., Shi, G., Wang, S., Wang, Y., Sun, Y., and McElroy, M. B.: Fine-particle pH for Beijing winter haze as inferred from different thermodynamic equilibrium models, *Atmos. Chem. Phys.*, 18, 7423-7438, 10.5194/acp-18-7423-2018, 2018.
- Squizzato, S., Masiol, M., Brunelli, A., Pistollato, S., Tarabotti, E., Rampazzo, G., and Pavoni, B.: Factors determining the formation of secondary inorganic aerosol: a case study in the Po Valley (Italy), *Atmos. Chem. Phys.*, 13, 1927-1939, 10.5194/acp-13-1927-2013, 2013.
- Tan, T., Hu, M., Li, M., Guo, Q., Wu, Y., Fang, X., Gu, F., Wang, Y., and Wu, Z.: New insight into PM_{2.5} pollution patterns in Beijing based on one-year measurement of chemical compositions, *Science of The Total Environment*, 621, 734-743, <https://doi.org/10.1016/j.scitotenv.2017.11.208>, 2018.
- Tao, Y., and Murphy, J. G.: The sensitivity of PM_{2.5} acidity to meteorological parameters and chemical composition changes: 10-year records from six Canadian monitoring sites, *Atmos. Chem. Phys.*, 19, 9309-9320, 10.5194/acp-19-9309-2019, 2019.
- Vieira-Filho, M., Pedrotti, J. J., and Fornaro, A.: Water-soluble ions species of size-resolved aerosols: Implications for the atmospheric acidity in São Paulo megacity, Brazil, *Atmospheric Research*, 181, 281-287, <https://doi.org/10.1016/j.atmosres.2016.07.006>, 2016.
- Wang, G., Zhang, R., Gomez, M. E., Yang, L., Levy Zamora, M., Hu, M., Lin, Y., Peng, J., Guo, S., Meng, J., Li, J., Cheng, C., Hu, T., Ren, Y., Wang, Y., Gao, J., Cao, J., An, Z., Zhou, W., Li, G., Wang, J., Tian, P., Marrero-Ortiz, W., Secrest, J., Du, Z., Zheng, J., Shang, D., Zeng, L., Shao, M., Wang, W., Huang, Y., Wang, Y., Zhu, Y., Li, Y., Hu, J., Pan, B., Cai, L., Cheng, Y., Ji, Y., Zhang, F., Rosenfeld, D., Liss, P. S., Duce, R. A., Kolb, C. E., and Molina, M. J.: Persistent sulfate formation from London Fog to Chinese haze, *Proc Natl Acad Sci U S A*, 113, 13630-13635, 10.1073/pnas.1616540113, 2016.
- Wang, H., Ding, J., Xu, J., Wen, J., Han, J., Wang, K., Shi, G., Feng, Y., Ivey, C. E., Wang, Y., Nenes, A., Zhao, Q., and Russell, A. G.: Aerosols in an arid environment: The role of aerosol water content, particulate acidity, precursors, and relative

Formatted: English (United States)

Field Code Changed

Formatted: English (United States)

Field Code Changed

Field Code Changed

Formatted: English (United States)

Formatted: English (United States)

Field Code Changed

humidity on secondary inorganic aerosols, Science of The Total Environment, 646, 564-572, <https://doi.org/10.1016/j.scitotenv.2018.07.321>, 2019.

Weber, R. J., Guo, H. Y., Russell, A. G., and Nenes, A.: High aerosol acidity despite declining atmospheric sulfate concentrations over the past 15 years, Nature Geoscience, 9, 282-285, 10.1038/ngeo2665, 2016.

Xue, J., Lau, A. K. H., and Yu, J. Z.: A study of acidity on PM2.5 in Hong Kong using online ionic chemical composition measurements, Atmospheric Environment, 45, 7081-7088, <https://doi.org/10.1016/j.atmosenv.2011.09.040>, 2011.

Yao, X., Ling, T. Y., Fang, M., and Chan, C. K.: Size dependence of in situ pH in submicron atmospheric particles in Hong Kong, Atmospheric Environment, 41, 382-393, <https://doi.org/10.1016/j.atmosenv.2006.07.037>, 2007.

Formatted: English (United States)

Field Code Changed

Formatted: English (United States)

Field Code Changed

Field Code Changed

Formatted: English (United States)